Journal Pre-proof

Implementation of bactericidal topographies on biomimetic calcium phosphates and the potential effect of its reactivity

Marc Iglesias-Fernandez, Judit Buxadera-Palomero, Joanna-Maria Sadowska, Montserrat Espanol, Maria-Pau Ginebra

PII: S2772-9508(22)00074-7

DOI: https://doi.org/10.1016/j.bioadv.2022.212797

Reference: BIOADV 212797

To appear in:

Received date: 15 November 2021

Revised date: 1 April 2022

Accepted date: 7 April 2022

Please cite this article as: M. Iglesias-Fernandez, J. Buxadera-Palomero, J.-M. Sadowska, et al., Implementation of bactericidal topographies on biomimetic calcium phosphates and the potential effect of its reactivity, (2021), https://doi.org/10.1016/j.bioadv.2022.212797

Implementation of bactericidal topographies on biomimetic calcium phosphates and the potential effect of its reactivity

Marc Iglesias-Fernandez[a,b], Judit Buxadera-Palomero[a,b], Joanna-Maria Sadowska[a,b], Montserrat Espanol[a,b,*] and Maria-Pau Ginebra[a,b,c]

[a]Biomaterials, Biomechanics and Tissue Engineering Group, Department of Materials Science and Engineering, Universitat Politècnica de Catalunya (UPC), Av. Eduard Maristany 16, 08019, Barcelona, Spain

[b]Barcelona Research Center in Multiscale Science and Engineering, Universitat Politècnica de Catalunya (UPC), Av. Eduard Maristany 16, 08019, Barcelona, Spain

[c]Institute for Bioengineering of Catalonia (IBEC), The Barcelona Institute of Science and Technology, Baldiri Reixac 10-12, 08028 Barcelona, Spain

ABSTRACT

Since the discovery that nanostructured surfaces were able to kill bacteria, many works have been published focusing on the design of nanopatterned surfaces with antimicrobial properties. Synthetic bone grafts, based on calcium phosphate (CaP) formulations, can greatly benefit from this discovery if adequate nanotopographies can be developed. However, CaP are reactive materials and experience ionic exchanges when placed into aqueous solutions which may in turn affect cell behaviour and complicate the interpretation of the bactericidal results. The present study explores the bactericidal potential of two nanopillared CaP prepared by hydrolysis of two different sizes of α-tricalcium phosphate (α-TCP) powders under biomimetic or hydrothermal conditions. A more lethal bactericidal response towards *Pseudomonas aeruginosa* (~75% killing efficiency of adhered bacteria) was obtained from the hydrothermally treated CaP which consisted in a more irregular topography in terms of pillar size (radius: 20-60 nm), interpillar distances (100-1500 nm) and pillar distribution (pillar groups forming bouquets) than the biomimetically treated one (radius: 20-40 nm and interpillar distances: 50-200 nm with a homogeneous pillar distribution). The material reactivity was greatly influenced by the type of medium (nutrient-rich versus nutrient-free) and the presence or not of bacteria. A lower reactivity and superior bacterial attachment were observed in the nutrient-free medium while a lower attachment was observed for the nutrient rich medium which was explained by a superior reactivity of the material paired with the lower tendency of planktonic bacteria to adhere on surfaces in the presence of nutrients. Importantly, the ionic exchanges produced by the presence of materials were not toxic to planktonic cells. Thus, we can conclude that topography was the main contributor to mortality in the bacterial adhesion tests.

1. INTRODUCTION

The use of synthetic bone grafts to treat bone defects resulting from trauma or diseases has helped millions of patients to improve their quality of life [1]. However, the complications derived from bone graft infection can be a serious health problem, resulting in delayed healing, graft failure and even death. The most common source of infection is the direct contamination of the wound and bone graft during surgery. In fact, orthopaedic treatments that require skin or mucosal breakdown or entry into a sterile body cavity, such as graft implantation or open fractures due to trauma, are considered to be at high risk of infection [2].

The most frequently isolated microorganisms in implant-related infections are Gram-positive *Staphylococcus aureus* and *Staphylococcus epidermidis*, although other strains such as Gram-negative *Escherichia coli* or *Pseudomonas aeruginosa* are also commonly detected [3,4]. When infection occurs, it starts with the attachment of bacteria to the implant surface, which in the worst case scenario leads to the formation of a biofilm, i.e. clusters of cells embedded in a protective extracellular polymeric substance (EPS) environment that shields the bacteria from the immune defence system, external physical stress, chemical biocides and antibiotics [3,5]. Even though the most common treatment to fight infection is through the administration of antibiotics [4,6], their limited penetration across biofilms [7,8] paired with the low vascularity of the infected/dead tissues [3] compromise their success. Moreover, an additional concern is the widespread development of resistant bacterial strains due to the excessive abuse and misuse of antibiotics [9,10]. Indeed, superbugs or multidrug resistant bacteria, like methicillin-resistant *Staphylococcus aureus* and *Pseudomonas aeruginosa* (*P. aeruginosa*), among others, pose a serious health threat that is expected to worsen in the future [9–11]. Therefore, there is a need to find alternative ways to fight infections without using antibiotics.

To date, several alternative strategies to the use of antibiotics have been proposed to prevent implant-associated infections. One of the most frequent strategies is to combine silver and its compounds with the desired material due to its broad-spectrum antimicrobial effects [12–15]. More recently, however, the design of bioinspired nanostructured bactericidal surfaces has emerged as a radically new strategy that relies on the ability of such topographies to lyse attached bacteria by physical mechanisms [16–18]. Due to a mechanical mechanism of rupture, surface topographies with patterns smaller than bacterial cells possess a potential universal bactericidal effect, regardless of the bacterial strain [19]. The bactericidal potential of contact-killing surfaces was discovered by

Ivanova et al. in 2012 on the wings of the cicada (*Psaltoda Claripennis*), consisting of nanopillars 200 nm tall, 60 nm in diameter and with an interpillar distance of 170 nm [20]. A year later, the same team successfully synthesized the first artificial bactericidal topography [21]. One of the main advantages of this approach is that bacteria are unable to develop resistance, and it is expected to have a more durable effect in the long term [22]. Additionally, with the exception of a few studies [23], eukaryotic cells can successfully colonize these nanostructured surfaces by accommodating the deformation stresses imposed by the nanopatterned substrates by invaginating the surface features, due to their larger dimensions and more elastic membrane.

While the precise mechanism responsible for the antibacterial activity remains a matter of debate, one of the most widely accepted model predicts that the bactericidal action comes upon bacterial adhesion by the excessive stretching of the cell membrane in the regions suspended between pillars, where the deformation is greater than at the site of adhesion itself [24]. Most bactericidal topographies are based on "protrusions" such as nanopillars, nanowires, nanocolumns, nanocones, nanoneedles, nanospikes, etc. and their bactericidal efficacy can be optimized by suitably tuning the height, tip diameter, spacing (density) and pillars elasticity of their respective surface features to promote the largest stretching degree of the bacterial membrane [17,18]. Nevertheless, the efficiency also depends on the bacteria cell wall thickness, owing to the difference in the micro mechanical properties and surface chemistry of the cell wall in different bacterial species [18]. To date, several studies have reported on the nanotopographical action of different surfaces on bacteria. However, only some of the work has been done on biocompatible materials (titanium, titania, gold, zinc oxide and some polymers like polymethylmethacrylate, gecko skin replicas made of alginate, and silk fibroin) and, to the best of our knowledge, none on synthetic bone grafts [25–30]. Indeed, being able to endow synthetic bone grafts with bactericidal properties, in addition to having osteogenic or even osteoinductive properties, would be of great impact.

An ideal synthetic bone graft should induce bone regeneration of the defect site [1]. Calcium phosphates (CaP) are particularly suited for this application due to their close similarity to the bone mineral phase, which gives them the capacity to rebuild damaged bone [31,32]. This contrasts with metallic implants which, despite having the ability to also bind to bone, are intended to replace damaged bone rather than stimulate regeneration. Calcium orthophosphates, when synthesized at low temperature, such as those involved in the processing of CaP cements and biomimetic precipitation, can efficiently lead to nanotopographies consisting of nano-size needles, rods and

plates that provide great benefits from the point of view of their osteogenic/osteoinductive potential [33–35]. Despite the ease with which nanostructured substrates can be prepared, little work has focused on studying the biocidal potential of such nano-topographic structures, being CaP coatings on titanium implants the closer application found in the literature to date [36]. Interestingly, some studies have investigated nanostructured CaP coatings not for the biocidal potential of their topography, but for the ability of these coatings to release biocidal agents by exploiting their high specific surface area [37,38]. This makes the investigation of potential nanotopographies in CaP a largely unexplored field.

But working with nanostructured CaP involves a property that most of the previously reported nanostructured bactericidal surfaces do not share, reactivity. Indeed, CaP, and in particular hydroxyapatite, is known to be a bioactive material with the ability to chemically bind to bone. This property is triggered by surface ionic reactions between the material and the surrounding medium, which ultimately lead to binding to bone [39]. In vitro cell culture studies of nanostructured CaP with eukaryotic cells have demonstrated that reactivity could dramatically affect cell behaviour, but without any visible change in the microstructure of the material [40,41]. We expect that, since Ca and P are essential nutrients for bacteria, ionic exchanges, in addition to the effect of nanotopography, may play a role in the final bactericidal response of nanostructured CaP.

Thus, the aim of this work is to explore the bactericidal properties of different nanopillared hydroxyapatite surfaces prepared by hydrolysis of alpha-tricalcium phosphate (α-TCP) under different conditions. Specifically, α-TCP powders are consolidated under biomimetic or hydrothermal conditions (biomimetic: immersed in water at 37.5ºC, atmospheric pressure; hydrothermal: immersed in water at 121ºC and 2 atm pressure) to adjust pillar size, diameter and interpillar distance. As a control, a flat and smooth surface is obtained by grinding and compacting one of the nanopillared substrates. In addition, the reactivity and antimicrobial potential of the different substrates is evaluated in two media: phosphate buffer saline and Luria broth, to assess if there is any effect/synergy between the bactericidal potential and the reactivity of the material. *P. aeruginosa* is used as the bacterial strain, as it has been widely explored in the investigation of mechano-bactericidal surfaces.

2. MATERIALS AND METHODS

2.1. Powder preparation

α-TCP was synthesized mixing calcium hydrogen phosphate ($CaHPO_4$, Sigma-Aldrich, St. Louis, USA) and calcium carbonate ($CaCO_3$, Sigma-Aldrich, St. Louis, USA) in a 1:2 molar ratio respectively. The mixture was sintered for 15.5 h until 1400ºC and quenched in air at room temperature to retain the high temperature α-phase. The obtained solid was then milled in an agate planetary ball mill (Fritsch, Pulverisette) following two different procedures to obtain powders with coarse (C: 5.2 μm median size) and fine (F: 2.8 μm) particle size. C powder was milled during 15 min at 450 rpm with 10 agate balls (30 mm diameter) and F powder was milled during 40 min at 450 rpm with 10 agate balls (d=30 mm), then for 60 min at 500 rpm with the same agate balls and finally for 60 min at 500 rpm with 100 agate balls (d=10 mm). After milling, F and C powders were mixed with a 2 wt.% of precipitated hydroxyapatite (pHA, Merck 2143, Merck, Darmstardt, Germany). The C powder was further sieved with a 40 μm sieve (Filtra, Spain) and the powder >40 μm was kept to further prepare the samples.

2.2. Sample preparation

Three different samples were elaborated consisting of: coarse nanopillared topography, fine nanopillared topography and a flat sample derived from a fine nanopillared topography. Samples were processed differently according to the desired topography:

- Coarse nanopillared discs of 5 mm diameter by ~1.1 mm height were elaborated from C powder by compacting 50 mg of powder at a pressure of 2 tons for 2 min (Atlas™ Manual Hydraulic Press, Specac). The discs were subsequently immersed in water (~20 μ per disc) and hydrolysed by hydrothermal treatment (autoclave) at 121ºC and 2 atm for 30 min. The samples were coded as H (hydrothermally treated) discs.

- Fine nanopillared discs of 5 mm diameter and ~1.1 mm height were elaborated from F powder by compacting 50 mg of powder at a pressure of 2 tons for 2 min (Atlas™ Manual Hydraulic Press, Specac). The discs were subsequently hydrolysed by immersing them in ~20 mL of water for 7 days at 37.5°C (biomimetic treatment). The samples were coded as B (biomimetically treated) discs.

- Biomimetic flat (BF) samples were prepared by first hydrolysing F α-TCP powder by immersion in water for 7 days at 37.5°C (biomimetic treatment) and subsequently the

powder was dried and pressed as earlier explained to get disks of 5 mm diameter by ~1.1 mm height.

All these reactions are based in the hydrolysis of α-TCP to calcium deficient hydroxyapatite (CDHA) according to the reaction:

$$3\ Ca_3(PO_4)_2 + H_2O \rightarrow Ca_9(HPO_4)(PO_4)_5(OH) \qquad \text{(Equation 1)}$$

2.3. Physico-chemical characterization

2.3.1. Microstructural characterization

The morphology and topography of the surface and cross-section of the discs was observed under a field emission scanning electron microscope (FESEM JEOL JSM7001F, Toyo, Japan) operating at 5 kV. Previously, the samples were carbon-evaporated to minimise charging effects (K950X Turbo Evaporator, Emitech).

Image analysis was performed to determine the distributions of the distance between crystals, the crystal radius, the crystal height, and the crystal orientation with respect to the surface. Pillar density and surface skewness were also measured. The value of skewness was used to indicate if the surface tended toward having more high narrow peaks with broader valleys (positive skewness), while negative skewness indicated a tendency to broader peaks with deep and narrow valleys [42]. These values were obtained from 3 different micrographs of each sample type. The different topographies were analysed using the software Gwyddion 2.59. Statistical differences in surface skewness and pillar density between samples were calculated using Welch t-test in Prism GraphPad.

2.3.2. Phase composition

The phases constituting the samples were identified by X-ray powder diffraction (XRD) and Fourier transform confocal laser Raman spectrometry.

The diffractometer (D8 Advance, Brucker, Karlsruhe, Germany) equipped with a Cu Kα X-ray tube and a primary monochromator was operated at 40 kV and 40 mA. The data collection set up was 0.02 steps over 10-60º with a counting time of 2s per step. Prior to analysis the samples were manually crushed in an agate mortar. Phase quantification was performed by Rietveld refinement

using the Profex software (Profex 4.3.5) [43]. Crystalline models for CDHA and β-TCP were taken from ICDD PDF 01-086-1201 and ICDD PDF 00-003-0681 respectively.

An inVia™ Qontor® confocal Raman microscope (Renishaw Centrus 2957T2, Gloucestershire, UK) was used for the characterization of the surface of each sample type. Spectra were acquired with lasers with a power of 150 mW, wavelengths of 532/785 nm and a grating of 2400/1200 l/mm were used respectively. Spectra were acquired with an objective of 100x, and 40 accumulations of 1s each. To assess repeatability, three random measurements were taken per sample.

2.4. Antimicrobial activity

2.4.1. Bacteria cultures

Pseudomonas aeruginosa (*P. aeruginosa*, CECT 110, from the Colección Española de Cultivos Tipo, Valencia, Spain) was used in the different antibacterial essays. Luria-Broth Base (Miller's LB broth base™-, powder, Thermo Fisher scientific, ref. 12795-027) was used to grow the inoculums.

2.4.2. Sample sterilization

For sample sterilisation the samples were first immersed in water and autoclaved at 2 atm of absolute pressure and 121ºC for 30 min. This was done with the double purpose of sterilising the samples and ensuring complete wetting of the samples (i.e., removal of the air entrapped between nanopillars that could lead to a misleading antifouling effect [44]).

2.4.3. Bacteria adhesion

Bacteria were overnight cultured in LB broth at 37.5ºC. The next day, cultures were centrifuged at 4000 rfc for 10 min to separate bacteria from the media. Cells were then resuspended in either LB or phosphate-buffered saline (PBS) solution (PBS tablets, Gibco®, ref. 18912- 014, lot 2153555) and their optical density (OD_{600}) adjusted to 0.25. Sterile discs were transferred to 48-well plates and inoculated with 0.7 mL of each suspension for 1.5 h, 4 h and 24 h at 37.5ºC. After each time point, discs were removed from the well plate and gently rinsed by submerging into wells pre-filled with PBS. This was repeated twice before fixation with 2.5% glutaraldehyde solution in PBS for 15 min in the fridge. Upon fixation the samples were washed with PBS thrice and stained using a live/dead bacterial viability kit (LIVE/DEAD® BacLight™ Bacterial Viability Kit, for microscopy, Cat. No. L7012, Molecular Probes, Invitrogen, USA). For this, 2.5 µL of the mixture 1.67 mM SYTO9/18.3 mM Propidium iodide was diluted in 1 mL of PBS and 500 µL of this solution was

added to the discs. After 7 min of incubation at room temperature in the dark, the discs were washed three times with PBS, and the samples imaged in a confocal laser microscope (Zeiss LSM 800, Germany). The samples were kept wet during imaging. Two independent lasers (488 nm and 561 nm) and band-pass filters for each fluorophore were used in the receptor region of 410-546 nm for SYTO9 and 600-700 nm for propidium iodide (PI) to not to have overlapping between green and red fluorescence. Three independent experiments were performed to confirm the consistency of results. In addition, a minimum of 3 images were taken per sample condition.

Zen Blue 2.3 ~~lite~~ (Zeiss Microscopy) software was used to acquire and analyse the fluorescent confocal images. Cells stained in green (SYTO 9) were considered viable and cells stained in red (propidium iodide) or with a superposition of both fluorophores were considered to have a damaged membrane. Statistical comparisons between samples and time points were based on one-way ANOVA and statistically significant differences were considered if the p value was less than 0.05 (Minitab18^{TM} software, Minitab Inc.). Different graphs were plotted reporting the average percentage of dead bacteria over the total adhered population (read area/total covered area) [%] and the total covered area [%].

After confocal observations, the samples were dehydrated by washings through a graded sequence of aqueous ethanol (PanReac Applichem. Lot 0000936500) solutions (50%, 70%, 90%, 96% and 100% twice) for 10 min and finally dried overnight at room temperature for examination under FESEM.

2.4.4. Reactivity tests

2.4.4.1. Evaluation of the materials' reactivity

The reactivity of the samples was assessed by measuring the Ca and P concentration by inductive coupled plasma-mass spectroscopy (ICP-MS, Agilent 7800 ICP - MS, CA, USA). To assess the ionic exchanges due to the material reactivity, discs were placed in a 48-well plate and incubated with 1 mL of LB or PBS. For the assessment of the ionic exchanges in the presence of bacteria, discs were immersed in 1 mL of *P. aeruginosa* at a OD_{600} of 0.25 in LB or PBS. In all the cases the discs were incubated at 37.5ºC for 24 h to maximize chemical activity. As controls, PBS and LB with/without *P. aeruginosa* were measured. Upon incubation all supernatants were filtered with a 0.22 μm pore size PES membrane (Millex-GP PES, Millipore) and 200 μL of the filtered solution was diluted in 2.3 mL of a 2% nitric acid solution (Nitric Acid 69% TMA, HIPERPUR, Panreac)

prior to ICP-MS quantification. Three samples were measured per condition. For the ICP measurements 44Ca and 31P signals were calibrated against a multi-element standard solution (Inorganic Ventures, USA). pH measurements were recorded using a selective electrode (CRISON INSTRUMENTS, MultiMeter MM 41).

2.4.4.2. Effect of materials' reactivity on planktonic bacteria growth

To determine if the reactivity of the samples with the medium could compromise the viability of planktonic bacteria, bacterial growth curves were monitored under the following conditions:

a) 100 µL of the filtered supernatants that were obtained in the previous section from incubation of the samples in either LB or PBS for 24 h at 37.5ºC were supplemented with 100 µL of a bacteria inoculum diluted to 10^7 and 10^4 cfu/mL and placed in a 96-well plate to monitor bacterial growth.
b) 100 µL of the filtered supernatants from the previous section that were obtained from incubation of the samples with *P. aeruginosa* either in LB or PBS for 24 h at 37.5ºC were supplemented with 100 µL of a bacteria inoculum diluted to 10^7 and 10^4 cfu/mL and placed in a 96-well plate to monitor bacterial growth.

In each experimental condition, a positive control was used consisting in 100 µL of bacteria inoculum (*P. aeruginosa* in LB) with 100 µL of fresh LB or PBS depending on the experimental condition. As negative controls 100 µL of LB was mixed with either 100 µL of LB or PBS. All bacteria inoculums were grown in LB at 37.5ºC for 24 h prior to experimentation and centrifuged to 4000 rfc for 10 min to separate the bacteria from the old media. For the quantification of the growth curves an absorbance measurement was made every 15 min at λ = 600 nm using a Synergy HTX Hybrid Multi Mode Microplate Reader (BioTek Instruments, Inc.).

3. RESULTS AND DISCUSSION

3.1. Physico-chemical characterization

The present study sets out to understand how the surface topography of calcium phosphates can be used to combat bacterial infection. Different nanopillared surfaces were prepared taking advantage of the hydrolysis of α-TCP into calcium deficient hydroxyapatite (CDHA) (Eq. 1) (**Figure 1**).

The surface topography of CDHA can be easily tuned by changing the size of the α-TCP and the consolidation/hydrolysis route (biomimetic: 37.5ºC / 1 atm *versus* autoclave: 121ºC /2 atm) as observed in **Figure 1**. Indeed, scanning electron micrographs showed that B discs -prepared using fine (F) powder consolidated under biomimetic conditions- resulted in a topography made of a dense network of fine pillars of nanometric size growing perpendicular to the disk surface. H discs instead, -prepared using coarse (C) powder consolidated in an autoclave-, led to the formation of taller pillared coarse crystals, which clustered together leaving large pocket-like structures between clusters. For comparison purposes a flat CDHA surface was also prepared compacting the biomimetically consolidated F powder (BF-Fine flat in **Figure 1A**). A closer look into the BF surface microstructure (inset image) allowed distinguishing the individual crystals.

The ability of CDHA to consolidate as small or larger pillars is tightly connected to the reactivity of the powder, which depends on the available surface area for reaction (specific surface area) and the consolidation conditions [45]. Depending on both, reactivity of the reagents and consolidation conditions, different supersaturation degrees can be achieved at a given temperature which, will ultimately control the crystallization process [46]. Indeed, the larger the surface area of the more energetically milled F α-TCP powder favors a high concentration of dissolved species (high supersaturation) and the formation of many nucleation points. When this is paired to a low temperature consolidation route (i.e., biomimetic) the process of crystal growth results in the development of finer and smaller CDHA crystals compared to a high temperature consolidation route. Conversely, the larger the size of α-TCP is connected to a lower concentration of ionic species which results in the formation of lesser nucleation points and the development of larger CDHA crystals. Indeed, it has been reported that the consolidation of C powder at 37.5ºC results in the formation of large crystal plates [33]. Nevertheless, by combining the low dissolution ability of C powders with a high temperature consolidation route, as it is achieved in the autoclave process, we can form clustered pillars of larger dimensions. Similar findings have been recently reported by Raymond *et al.* [47].

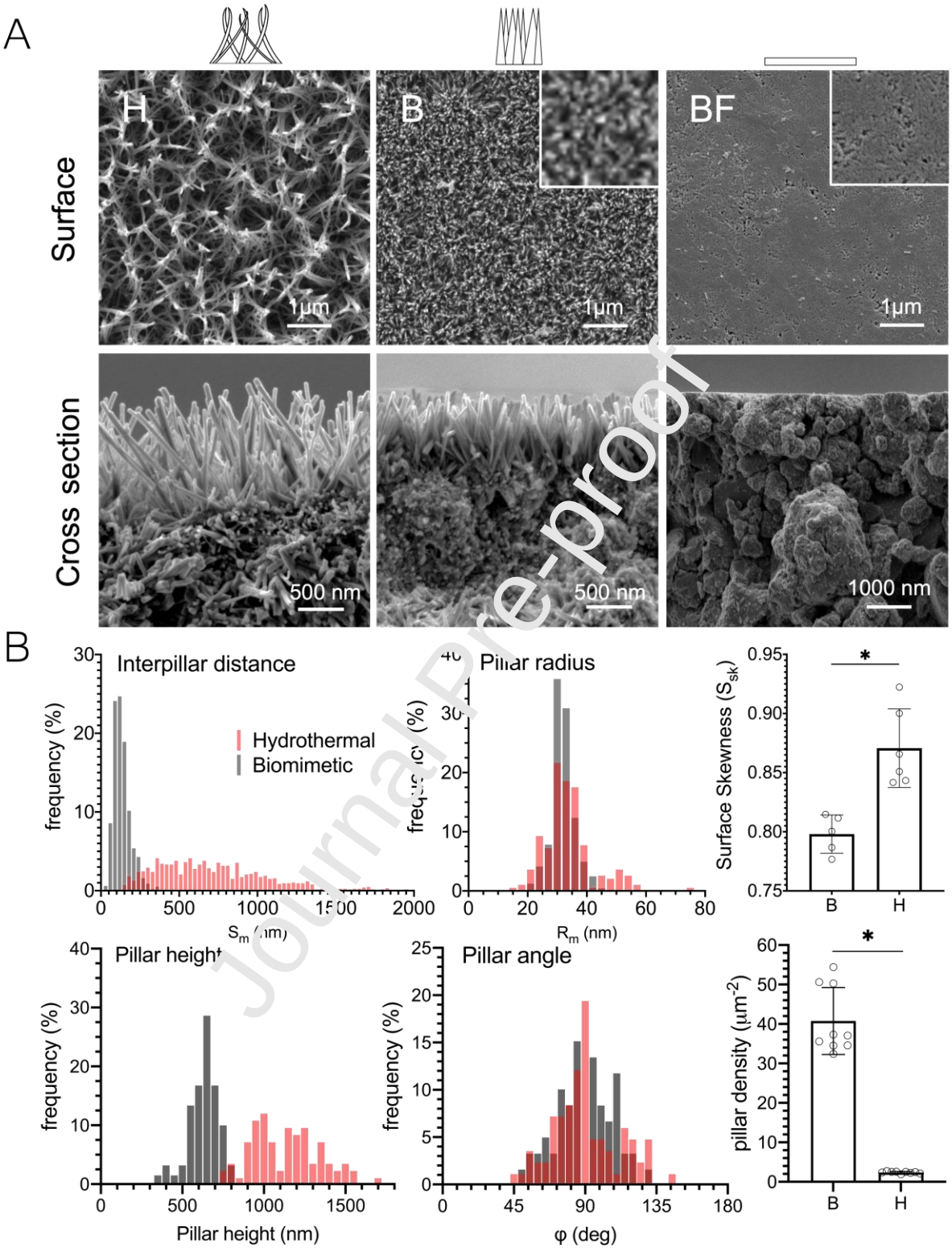

Figure 1. a) SEM micrographs showing the surface topography (top row) and cross-section of the samples (bottom row); b) Histograms of the inter-crystal distances (interpillar distance), pillar radius, pillar height and pillar orientation with respect to the surface for the hydrothermal (H) and biomimetic (B) topographies. Surface skewness and pillar density for the H and B samples are also plotted. '' indicates significant differences between samples ($p<0.05$) analyzed with a Welch t-test.*

To quantify the major characteristics between H and B microstructures, image processing analysis were performed (**Figure 1B**). The more homogeneous and densely packed microstructure observed in the B discs tended to an intercrystalline distance of ~100 nm which contrasted with the wider range of intercrystalline distances observed in the H discs that spanned from 100 to 1500 nm. Similarly, B discs presented a narrower size distribution in terms of the needle radius centered at ~30 nm (radius range 20-40 nm) while a wider range in pillar radius were obtained in the H discs, i.e., 20-60 nm. In terms of crystal height, the B crystals grew up to ~640 nm perpendicular to the disc surface, while H pillars exceeded twice this height. Along the same line, the spectrum of needle heights was broader in H, spanning from 700 to 1600 nm, than in B, which was narrower and more homogeneous. The orientation of the pillars, as expected, was predominant in the vertical direction on both topographies, but deviations up to ±45º were found. Globally, the topographical features of H and B align with the recently published characteristics that nanopillared surfaces should present to kill bacteria [48]. Indeed, Cui *et al.* concluded after screening of 12 different regular and well-controlled pillared topographies formed on polycarbonate, that the highest bactericidal rates were obtained from topographies consisting of pillars above 200 nm height, less than 60 nm of pillar diameter and around 170 nm interpillar spacing. These values closely matched the topographical features of *Psaltoda cleripennis* wings onto which it was discovered the bactericidal action of nanotopographies [20]. However, extrapolation of these values to our CDHA is not straightforward as differences may appear depending not only on the material but also on experimental conditions and methodologies (bacterial type/strain, culture medium, etc.) [49].

Further analyses in terms of skewness (Ssk) were performed to quantify the surface properties of the samples [50]. S_{sk} is used as a sensitive measure of the degree of asymmetry of the height distribution about a mean surface level. Positive values for skewness indicate if a surface tend toward having more high narrow peaks with broader valleys, while negative skewness indicates a tendency to have broader peaks with deep and narrow valleys. As expected, the obtained results (**Figure 1B**) showed that both B and H had positive skewness as both topographies consisted of peaked topographies. By comparing the values obtained, H topography had statistically significant greater skeweness than B. This implied that the H topography was less dense than B despite its intercrystalline distance distribution overlapped B values.

The works available in the literature concerning the use nanostructured surfaces with bactericidal properties assume inert, unreactive surfaces. But nanostructured CaP are inherently reactive. The

degree of reactivity depends on the type of CaP that develops during the consolidation of the samples. To determine the composition of H and B discs X-ray diffraction (XRD) and Raman spectroscopy analysis were performed (**Figure 2**). The measurements were taken from the surface of the discs. In line with other reported works the results showed that the hydrolysis of α-TCP under biomimetic conditions (B and BF samples) mostly consisted of CDHA (>96 wt%) and a small fraction of β-TCP (<4 wt%). This later phase is believed to be stabilized during the quenching process of α -TCP due to the presence of impurities or to an insufficient cooling rate [51]. Additionally, Raman results confirmed the presence of the typical vibrational bands for the PO_4^{3-} and HPO_4^{2-} groups in CDHA [52,53] as indicated in **Figure 2B**. The major difference of the H samples consolidated in the autoclave compared to the biomimetically consolidated ones, can be seen in the greater proportion of β-TCP (β-TCP=39%wt and CDHA=61%wt) detected by XRD. The stabilization of β-TCP has been commonly reported when α-TCP is hydrolyzed in an autoclave [54] and although it is not well understood why this phase is formed, its stabilization is favored by the application of pressure in the process. Interestingly, Raman spectroscopy results performed on the H samples did not show bands attributable to the β-TCP phase which was explained from the fact that the beta phase was not exposed to the sample surface but was located within. This is in line with other published works [55]. Only X-Rays, capable of penetrating underneath the surface were thus capable of detecting β-TCP during the analysis.

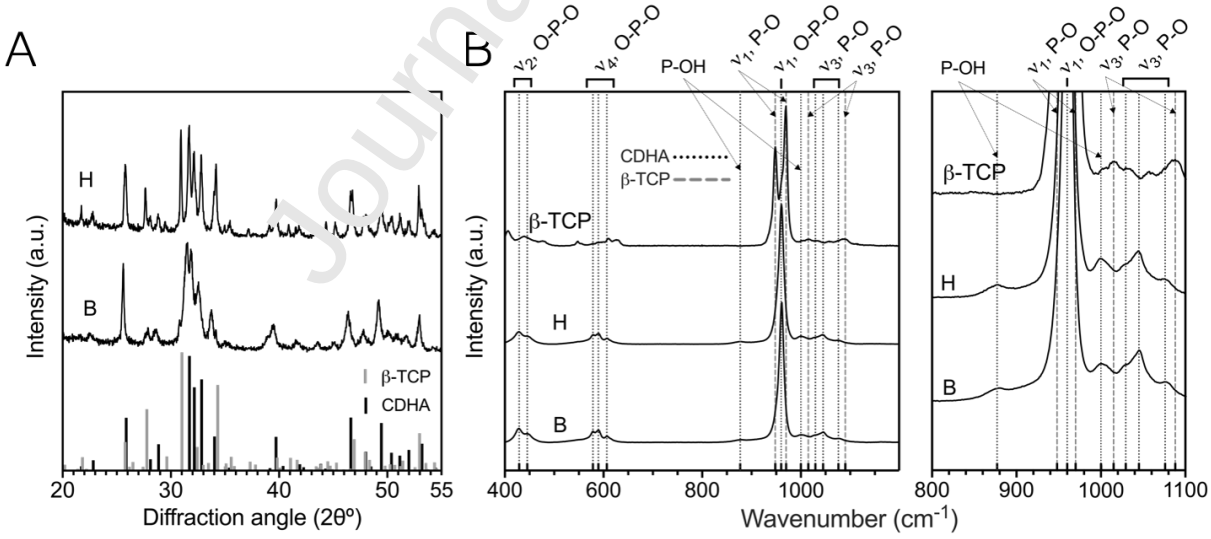

Figure 2. a) XRD patterns and b) Raman spectra of the different calcium phosphate substrates. The vertical lines at the bottom of the XRD graph represent CDHA and β-TCP peaks obtained from PDF 01-086-1201 and PDF 00-003-0681 respectively. The vertical dotted lines in the Raman spectra indicate the vibrational modes and their respective molecular bonding.

Overall, the analysis of the B and H samples resulted in different nanopillar structures with single-phase and two-phase composition. Although compositional differences could complicate the interpretation of the effect of topography, it has been shown that, in terms of *surface* composition, both B and H nanopillars were composed solely of CDHA. However, the overall reactivity of the sample could still be affected due to the diffusion of ions through the sample. The contribution of reactivity and its effect on bacteria will be tackled in sections 3.3 and 3.4.

3.2. Antimicrobial activity

The antibacterial efficacy of the different surfaces was assessed by an adhesion-based assay, which is typically suited for evaluating contact-killing designs [18]. The relative proportion of dead cells and the total number of adherent cells on the different substrates was assessed using Live/Dead Viability Kits which demonstrate the viability of bacteria by the absence or presence of bacterial wall damage. Cells with intact cell membrane were stained green (SYTO 9) and were considered viable cells and cells with compromised membrane were stained red (propidium iodide, PI) and were considered dead. This makes Live/Dead kit an interesting assay to evaluate the bactericidal efficacy of a topography, as this method reflects the integrity of the cells membrane, which is precisely the mechanism by which a bacterial cell dies by a topography-mediated effect [56]. Additionally, in the preparation step of the samples prior to the cell culture, care was taken to ensure complete wetting of the surface before contacting the bacterial suspension with the substrates. Indeed, the presence of air entrapped between pillars can restrict the available area for bacterial adhesion leading to an antifouling effect and misleading results [44]. This issue was solved by subjecting the samples before analysis, to an autoclave cycle in which the samples were immersed in water with the double purpose of eliminating air bubbles and sterilization. Moreover, the bactericidal potential of the different CaP was evaluated using two different media: a nutrient depleted medium (phosphate buffer saline, PBS), and a nutrient rich medium (Luria broth, LB). PBS medium was chosen to evaluate the viability of bacteria on the nanotopographies over time, ensuring that the attached population undergoes minimum changes in number from the start of the experiment. LB medium was chosen to evaluate the bactericidal potential of the topographies in an optimal environment for bacteria in which they can thrive comfortably and proliferate, implying an increment in the population since the beginning of the experiment.

3.2.1. Bacterial adhesion in phosphate buffer saline

Figure 3 shows the bactericidal effect of the developed CDHA surfaces at different time-points using *P. aeruginosa* in phosphate buffer saline (PBS). PBS was used to create an oligotrophic habitat, that is an environment depleted of nutrients to halt bacteria replication. This was of interest in our experiments to assess the bactericidal properties with a stable cell population throughout the duration of the experiment. The lack of nutrients did not suppose a problem for the viability of *P. aeruginosa*, which are able to persist under nutrient-poor conditions [57], including long-term survivability in PBS [58]. This was confirmed adding glass coverslips in our experiments which showed a level of mortality equivalent to other studies in rich-nutrient media [29,59,60]. Moreover, the strategy of working in nutrient depleted medium such as PBS has been widely used by many authors [23,61–66]. Nevertheless, bacteria responds to starvation reducing the cell size during the so-called "dwarfing" phase, whereby the cell undergoes metabolic and structural organization to resist starvation [67]. This explains the progressive reduction of the cell volume observed in the live/dead confocal images of viable bacteria with incubation time (**Figure 3**).

The behavior of *P. aeruginosa* on the different substrates confirmed the bactericidal potential of the CDHA nanopillar substrates. Indeed, images from live/dead staining showed that the average bactericidal activity was greater on the pillared topographies (B and H) than on flat topographies (BF and glass coverslip) at all time points and at 24 hours the bactericidal effect of the C pillars was greater than any other topography. In fact, on C samples almost half the cell population was already dead after 1.5 h and 70% after 24 h. On F samples ~40% of the population died at 1.5 h and a 60% after 4 h. These results were further confirmed by SEM where the micrographs showed extensive cell damage on B and H bacteria after 24 h (**Figure 4**). Importantly, the percentage of dead bacteria on the flat BF sample was always below 25%. However, the slight increment in bacterial mortality comparing BF with the ~15% of bacterial mortality on the control glass coverslips, points to an additional source of cytotoxicity -other than the mechano-bactericidal mechanism- which may relate to the reactivity of CDHA and will be addressed in the next sections. Of note, for all the conditions (B, H and BF), there were no significant differences in the percentages of total cell number amounting to approximately 15% of the total available surface. Table S1 and Figure S1 in the Supplementary Information compares the bactericidal action of our topographies with other reported works.

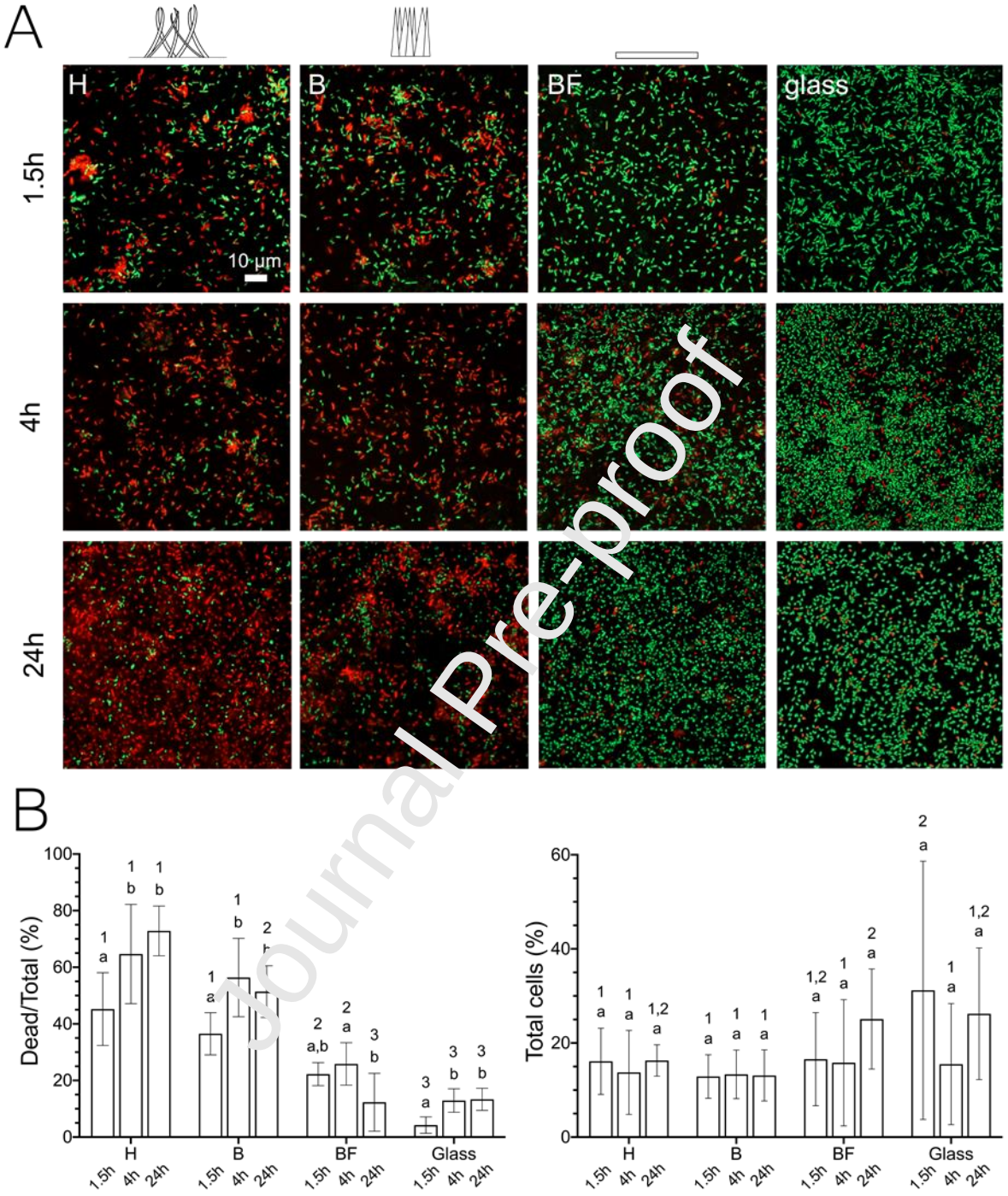

Figure 3. a) Representative CSLM images of P. aeruginosa adhered on the samples at the different time points. Bacteria were stained with Live/Dead BacLight. Red bacteria correspond to bacteria with damaged membrane, green bacteria correspond to viable bacteria. b) Quantitative analysis of the % of dead/total bacteria and % of bacterial coverage at 1.5, 4 and 24 h incubation on the different topographies. Quantitative data are expressed as mean ± standard deviation (n=9 from 3 independent experiments). Groups identified with the same superscripts are not statistically different ($p > 0.05$). Numbers identify differences between samples at each time point ($p < 0.05$), letters indicate differences between time points for the same sample type ($p < 0.05$).

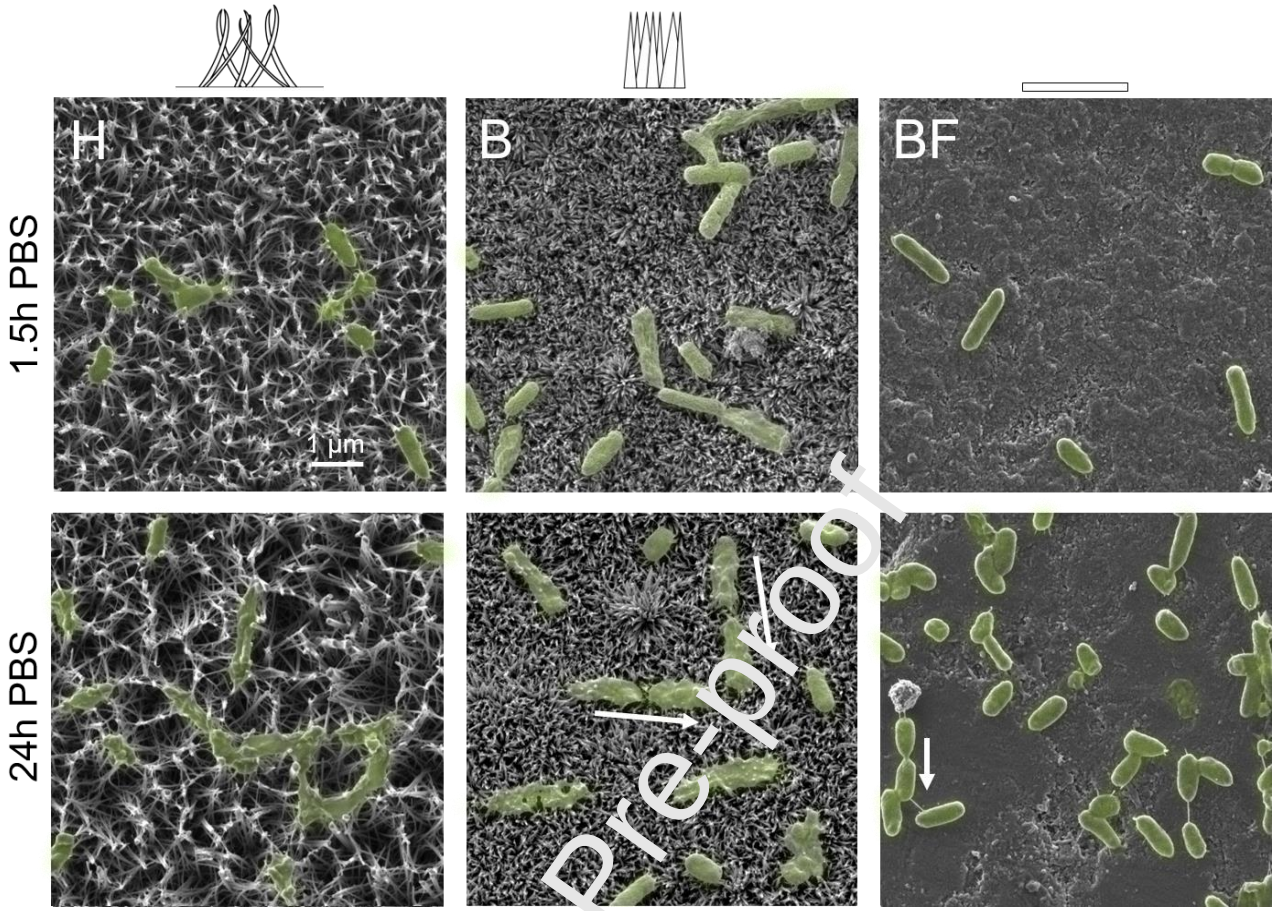

Figure 4. SEM micrographs of adhered bacteria inoculated in PBS on the different topographies. Notice the difference in bacteria with damaged cell wall which are flat and deformed and viable bacteria that maintain their rod-shaped morphology. Arrows indicate bacteria that had experience cell division.

The results thus far support the general finding that nanostructured materials can mechanically kill bacteria upon contact through physical forces (mechano-bactericidal) provided the surface possesses high aspect ratio pillars with appropriate dimensions and spacing. Given these premises two possible bactericidal mechanisms can operate [18]: the one involving stretching and tearing of the bacterial cell between nanopillars or by directly piercing the bacterial membrane. In any case, since the driving force for the mechano-bactericidal action is the physical attraction between the bacterial cell wall and the material, surfaces promoting strong adhesion forces should be more bactericidal. The less lethal behavior of B compared to H could be explained by a bed-of-nails effect in which the topography of B -thanks to its densely packed nanopillar structure- is able to more evenly distribute the force supported by the bacterial cell making membrane rupture more difficult. Improving the bactericidal effect of nanopillars is possible, but requires adjusting the height, tip diameter, interpillar distance and pillar density to stretch and rupture the bacterial membrane more effectively [68,69]. Unfortunately, there is still no consensus on the exact parameters for lysing cells. Regarding the pillar radius, for example, some studies argue that the

smaller the pillar tip, the greater the pressure that enhances lysis. However, other studies suggest that larger radius enhances the contact area between the bacteria and the pillar, leading to stretching of the suspended region of the bacterial membrane to accommodate the change in perimeter and, ultimately, rupture. Similarly, in terms of pillar density/spacing, an optimal range is needed. If the spacing is larger than the bacteria dimensions, bacteria would settle between pillars without experiencing any lysis effect, and if the spacing is too close, a bed-of-nails effect is produced.

Interestingly, SEM micrographs corresponding to B and BF (**Figure 4**) captured some bacteria after they had undergone cell division. It is not incompatible to observe a minimum of cell proliferation even when working under starvation conditions because of the storage of nutrients inside the cell. Thus, proliferating bacteria can be easily distinguished by their alignment, as cell division in rod-shaped bacteria occurs by in-plane elongation (arrows in **Figure 4**). The state of the cells in B was totally deflated indicating cell death. The images may point to an additional mechanism of cytotoxicity which occurs when well-adhered bacteria undergo cell division and, in the process, frictional forces between the cell membrane and the underlying nanopillars tears the cell wall [70]. Cell division in BF left the bacteria with their typical shape, indicating viability even after division, and thus in this case frictional forces did not cause membrane tearing. For this latter mechanism to work, apart from the presence of nanopillars, the bacteria must be firmly attached to the sample surface to create sufficient frictional forces to break the cell membrane [69,71].

One aspect that deserves consideration is to what extent the topography of nanopillars, lethal in bacteria, could damage the membrane of eukaryotic cells. The bactericidal nature of nanopillar surfaces is explained by morphological and structural differences between prokaryotic and eukaryotic cells. Since eukaryotic cells are larger than prokaryotic cells, the membrane perturbation caused by the nanoscale pillars is proportionally less significant for eukaryotic cells. In addition, the absence of the rigid peptidoglycan layer in eukaryotic cells makes them more flexible than prokaryotic cells, allowing eukaryotic cells to wrap around the nanostructured surface without rupturing [72,73].

3.2.2. Bacterial adhesion in Luria Broth

Figure 5 summarizes the live/dead staining results showing the bactericidal effect of the different substrates using *P. aeruginosa* in LB (nutrient rich environment). Unlike in PBS, working with LB

promotes unrestricted cell division and thus continuous bacterial growth until nutrient depletion. Although it could be argued that conducting experiments in LB has the advantage of being more physiologically relevant, it makes interpretation of the mechano-bactericidal action more difficult. Indeed, assessing the bactericidal potential in a condition where bacteria divide every 25-35 min is challenging, as the results may capture a population of alive bacteria adhered minutes before the completion of the experiment. But in any case, and considering this limitation, the results obtained were quite surprising. The most striking aspect was the low population of bacteria detected in all the substrates, nanopillared (B, and H) and flat (BF), for all the time points. Less than a 5% of surface coverage was obtained, which contrasted with the three-fold value observed in PBS. This was even more surprising when considering than in LB the cell population was substantially high due to continuous cell division.

One possible explanation to the limited attachment could be the presence of nutrients in the incubation medium. Indeed, bacterial attachment in nutrient-rich growth medium is known to be less favoured than in starving conditions [74]. This is because the presence of nutrients in suspension eliminates the need for planktonic bacteria to adhere seeking for an "accumulation of nutrients" on the sample surface [75]. However, the observation of a higher population of bacteria adhered on the glass coverslips incubated in nutrient rich medium (**Figure 5**) suggests that there could be additional explanations to this behaviour. Indeed, the inherent reactivity of CDHA coupled with the *P. aeruginosa*'s own metabolism can also play a role in bacterial attachment. CDHA is inherently reactive and capable of establishing ionic exchanges with the surrounding media fostered by the nanometric size of the crystals, their non-stoichiometry and poor crystallinity [40,41]. In fact, in many studies in which similar CDHA were cultured with eukaryotic cells, ionic exchanges in terms of Ca, Pi and pH changes were detected that significantly affected cell behaviour -this, without alteration of the materials' surface topography- [40,41]. In the case of bacterial cultures, and depending on the bacterial strain and culture conditions, ionic exchanges are also likely to occur, and may influence adhesion. Moreover, the bacteria's own metabolism could also play a major role. In fact, phosphorous is an essential component of core biological molecules and in bacteria, P is acquired mainly as inorganic orthophosphate. One particular case is that of phosphate solubilising microorganisms (PSM), where some Gram-negative bacteria, such as certain *P. aeruginosa* strains, have demonstrated the ability to hydrolyse organic and inorganic phosphorous compounds from insoluble sources when there is no available soluble P [76,77]. The principal mechanism for mineral phosphate solubilisation is the production of organic acids by bacteria.

These organic acids act through local acidification of the microbial cell and its surroundings and by chelation of divalent cations (e.g. Ca^{2+} from the substrate) resulting in CaP dissolution [57,78]. Although PSM could explain the limited bacterial adhesion by surface degradation, we do not expect PSM to play a major role due to the presence of P soluble salts in the formulation of the LB broth. This is indeed supported by the lack of changes (i.e., degraded surfaces) in the topography of the samples incubated with *P. aeruginosa* in LB when compared to the pristine substrates (**Figure 1** and **Figure 6**).

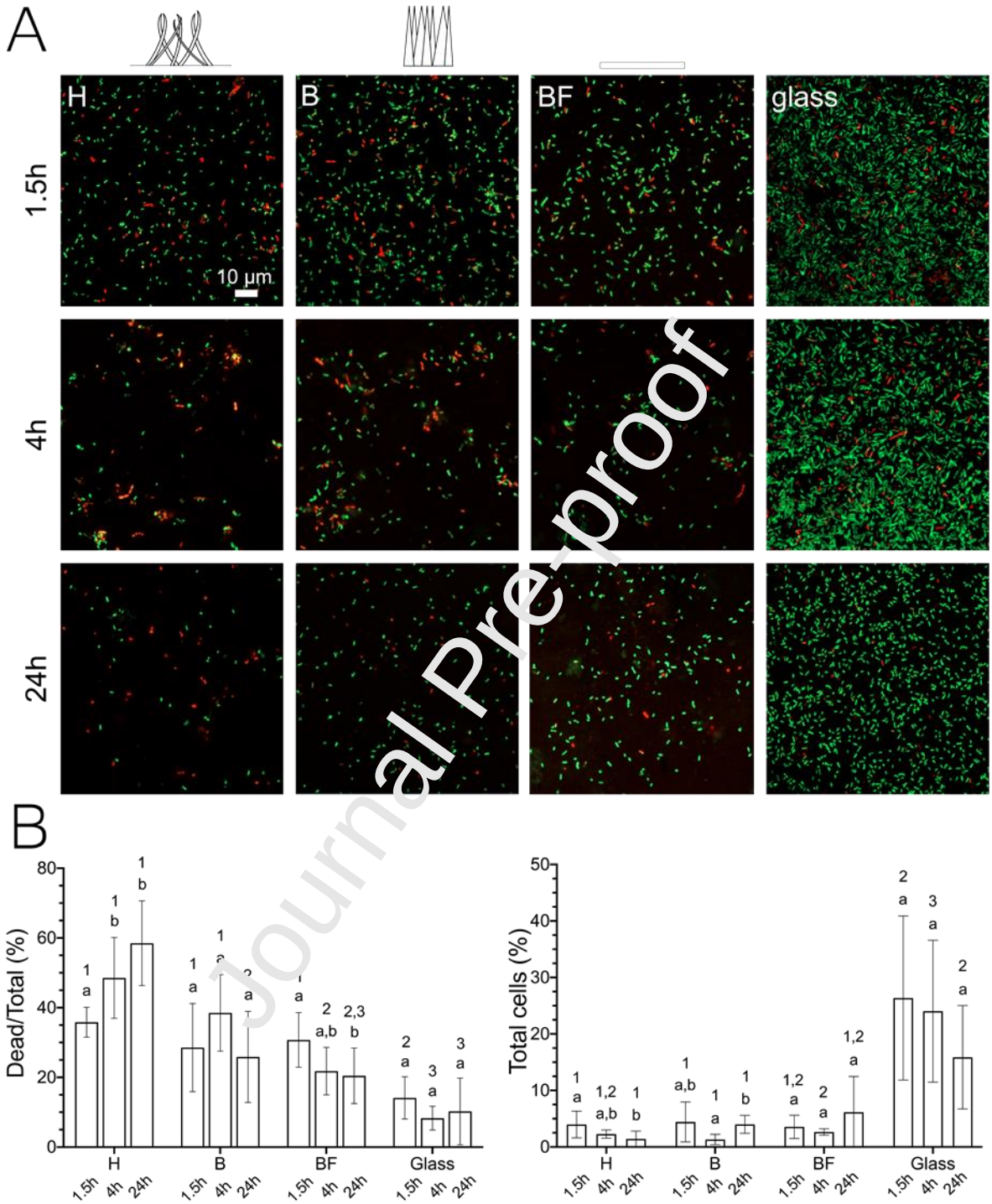

Figure 5. a) Representative CSLM images of P. aeruginosa adhered on the samples at the different time points. Bacteria were stained with Live/Dead BacLigth. Red bacteria correspond to bacteria with damaged membrane, green bacteria correspond to viable bacteria. b) Quantitative analysis of the % of dead/total bacteria and % of bacterial coverage at 1.5, 4 and 24 h incubation on the different topographies. Quantitative data are expressed as mean ± standard deviation (n=9 from 3 independent experiments). Groups identified with the same superscripts are not statistically different (p > 0.05). Numbers identify

differences between samples at each time point ($p < 0.05$), letters indicate differences between time points for the same sample type ($p < 0.05$).

In general, and despite the low bacterial population on the different substrates, H samples still showed the highest bactericidal potential. Nevertheless, no differences in bactericidal potential were found between B and BF, except at the 4 h time point, which is partly explained by the large dispersion in the measurements. SEM micrographs (**Figure 6**) allowed not only to confirm the damaged state of some of the bacteria adhered to the H and B surfaces but were also useful to rule out any sign of degradation of the samples. However, the contribution of ion exchange to bacterial adhesion remained to be revealed and to this end a detailed study of Ca, P and H concentrations in the absence and presence of *P. aeruginosa* was carried out and is presented in the following section.

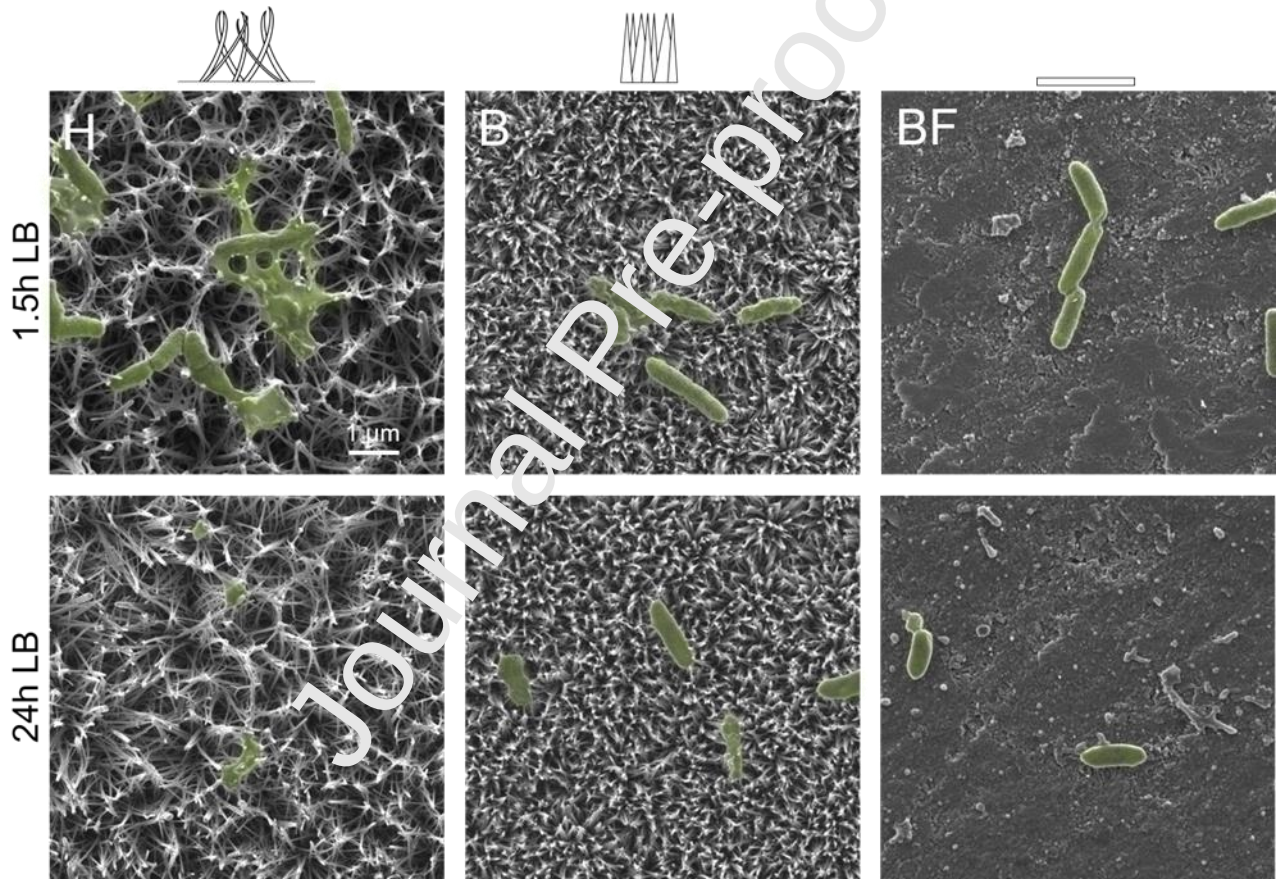

Figure 6. SEM micrographs of adhered bacteria inoculated in LB on *the different topographies. Notice the difference in bacteria with damaged cell wall which are flat and deformed and viable bacteria* that *maintain their rod-shaped morphology.*

3.3. Evaluation of material's reactivity

When CDHA are incubated into any solution (buffer, cell culture media, bacterial broth…), they can interact with their ionic environment in several ways, including crystal growth/precipitation, crystal dissolution and through ion exchange events between the media and the so-called hydrated layer of the material. The hydrated layer is described as a structurally ordered layer that develops on the surface of nanostructured crystals and consists in loosely bound ions that can be easily and reversibly substituted by other ions in fast aqueous ion exchange reactions [79,80]. Reactions across the hydrated layer are particularly relevant as they are both quick and easy due to the increased ionic mobility within the layer. In any case, all the above-mentioned reactions can potentially occur and affect cell interaction as had been widely demonstrated with eukaryotic cells [40,41,81].

We have evaluated the reactivity of the samples with the surrounding medium by quantifying by ICP the Ca and P concentrations. The different samples were incubated in PBS and LB, exactly as in the adhesion assay. The analyses were performed under the following experimental conditions: on the one hand, the samples were incubated in fresh PBS (**Figure 7a** left -white bars-) and in fresh LB (**Figure 7a** right -white bars-) to evaluate the intrinsic reactivity of the material with the surrounding medium, without bacteria. On the other hand, the samples were incubated in a bacterial inoculum diluted in PBS (**Figure 7a** left -orange bars-) and in LB (**Figure 7a** right -orange bars-) to evaluate the reactivity of the samples interacting with the possible changes that may take place in the presence of bacteria, in addition to the effect of the different compositions of the different media. The time point chosen was 24 h to maximize chemical activity. In addition, the pH values of the different suspensions were recorded.

Analysis of the Ca and P concentration of the samples incubated in PBS did not result in drastic changes when compared to the control (PBS) other than a global decrease in P and a slight release of Ca from the samples. The limited calcium dissolution was coherent with the low solubility of CDHA in the assayed conditions [82]. Globally, the results pointed that both, dissolution and sorption events simultaneously took place [83] without apparent changes of the surface microstructure (**Figure 7**). In the presence of bacteria, similar results (i.e., limited reactivity) were obtained which were attributed to the low bacterial metabolic activity in oligotrophic environments. However, the fact that in the presence of bacteria Ca was no longer detected in the suspensions incubated with samples (with the exception of H) could be explained by different reasons: a) the metabolization of this ion by the bacterial cells themselves [84] or its association with molecules secreted by the cells (divalent cations are known to intervene in the flocculation or gelation of

extracellular polymeric substances, EPS) [85,86] but also by b) the increase in pH due to the release of alkaloid metabolites from the bacteria causing a simultaneous reduction in the solubility of CDHA. Unfortunately, the current study does not allow determining which of these mechanisms prevails.

The pH increase observed in the presence of bacteria is supported by the wide range of external pH values in which non-extremophilic bacteria can grow (from 5.5–9), while keeping a cytoplasmic pH within the narrow range of pH 7.4-7.8 [87]. Furthermore, in the particular case of *P. aeruginosa*, pH has been found to increase markedly after infection in intestinal mucosa [88] and skin [89]. In addition, investigation of *P. aeruginosa* biofilm-mediated infection in synthetic calcium phosphate also led to an increase in pH [90]. All these results indicate that alkalinisation of the medium is not uncommon for *P. aeruginosa*, as it supports bacterial colonization and /or invasion. As previously mentioned, this rise in pH leads to a decrease in CDHA solubility, which explains the decrease in Ca^{2+} content observed in **Figure 7**.

Analysis of the results in LB media in the absence of bacteria indicated a superior reactivity of the samples as observed by the substantial increase in the Ca of the medium (at least for H and BF samples) despite the presence of soluble Ca and P in LB. Indeed, there was almost 10x more release of Ca from H samples in LB than in PBS (**Figure 7**) and 4x more release in the case of BF. We suspect that the lower pH of LB compared to PBS and the presence of organic molecules in the LB formulation with affinity for Ca^{2+} are responsible for the higher reactivity of the different materials in LB. However, this did not translate into an overall increase in the P content which indicated that complex dissolution/sorption reactions were occurring. In the presence of bacteria there was a substantial decrease in both Ca and P concentrations expectable for a copiotroph strain which requires of high levels of nutrients for growth. The need for Ca and P in the metabolism of a growing bacterium is what suggests the involvement of these ions during bacterial growth, however, the increased pH observed in the presence of bacteria decreases the solubility of CDHA, which should also result in a reduction of Ca and P ions in solution. We hypothesize that this reactivity, paired with the less favorable attachment of bacterial cells in nutrients rich medium could be the reason for the overall limited attachment. However, more in-depth studies are needed to fully disclose the role of reactivity in bacterial attachment.

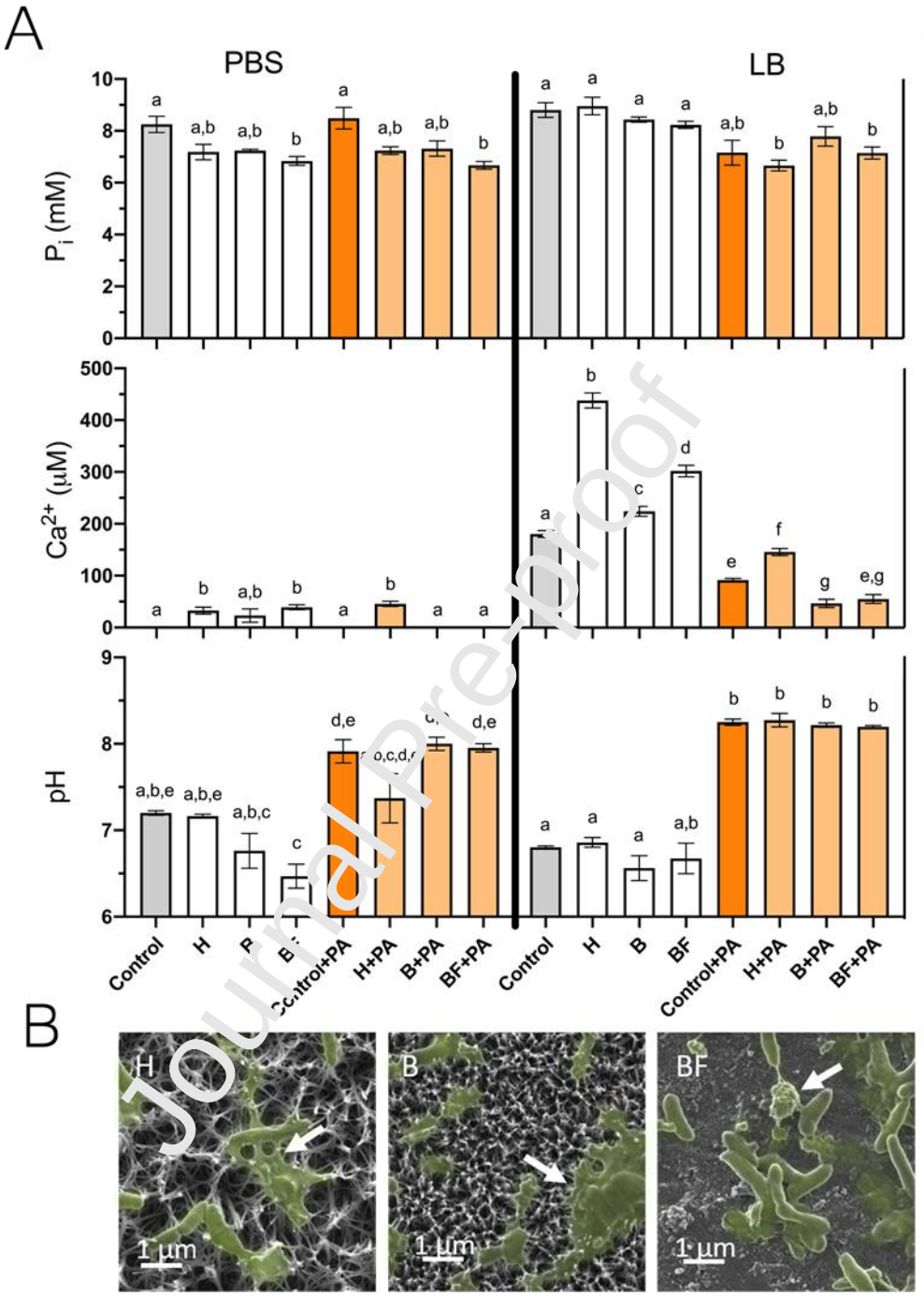

Figure 7. a) Quantification of phosphorus and calcium concentrations detected in PBS (white bars) and LB (orange bars) in presence (+PA, P. aeruginosa) or absence of bacteria by ICP-MS and H^+ determination by pH measurements. Controls correspond to pure media (PBS in grey color, LB in deep orange color). Bars represent means ± standard deviation (SD) of three samples. Groups identified with the same superscripts are not statistically different ($p > 0.05$). Letters indicate differences between conditions ($p < 0.05$). b) SEM micrographs showing with white arrows EPS (extracellular polymeric substances) production on the samples after bacterial incubation.

Moreover, as part of *P. aeruginosa*'s metabolism, there is secretion of hydrophilic extracellular polymeric substances (EPS) (**Figure 7b**) which have strong affinity for Ca. Since the Ca

sequestered during EPS development [85] is not taken into account in the ICP measurements as remains on the sample surface (**Figure 7b**), we expect in fact superior Ca releases, i.e. superior reactivity, than the levels detected by ICP. Interestingly, all these ionic reactions take place without alteration of the material's microstructure.

3.4 Effect of material's reactivity on planktonic bacterial growth

One question that arises when interpreting the bactericidal potential of reactive CaP is to what extent the chemical activity of the material is playing a role in the viability of planktonic bacteria. This is of interest to better understand the contribution of the physical properties and the chemical factors in the interpretation of the bacterial adhesion tests. To answer this question, the following studies were made. On the one hand it was explored if the supernatants obtained upon immersion of the samples in PBS/LB for 24h were toxic to *P. aeruginosa*. For this, a known amount of *P. aeruginosa* was added to the supernatant and the growth curve of bacteria was monitored with time (**Figure 8 a**). In addition, since the sample's reactivity is affected by the presence of bacteria, and bacteria itself can secrete metabolites that can influence bacterial growth, a similar experiment was done using the supernatant from samples incubated in LB/PBS in the presence of bacteria (**Figure 8 b**). This supernatant was subsequently filtered (to remove bacteria) before adding a known amount of fresh *P. aeruginosa* to monitor their growth curve. In case a supernatant was toxic to bacteria, a longer lag phase would be detected, which should be seen by a delay in the appearance of the exponential phase in that condition. As the lethality of a supernatant depends on the concentration of the toxins, two different concentrations of bacteria were tested in case a larger population of bacteria would be less sensitive to possible toxic effects, while a smaller population would be more lethal.

Analysis of the growth curves for the different conditions proved that none of the supernatants were toxic to the cells. This was inferred from the fact that the lag phase and the shape of the growth curves under any experimental condition did not differ between samples and positive controls for the same media and bacterial dilution. As expected, all conditions in which bacteria were incubated with LB reached greater levels of OD due to the greater amount of nutrients available. In contrast, the lower OD levels achieved when bacteria were supplemented in bacteria pre-cultured LB supernatants were due to nutrients uptake during pre-culture (**Figure 8** bottom right versus bottom left). From these results it is concluded that planktonic bacteria are not affected from the ionic

activity of the material neither from any of the released metabolites from bacteria. However, we cannot exclude that locally, on the surface of the H samples, where the highest concentration of ions accumulates, an increase in toxicity could be attained. In any case, the comparison of the bactericidal behaviour of the B and BF samples with identical composition guarantees the hypothesis that the main factor of mortality in the adhesion test is attributed to a physical effect of the topography.

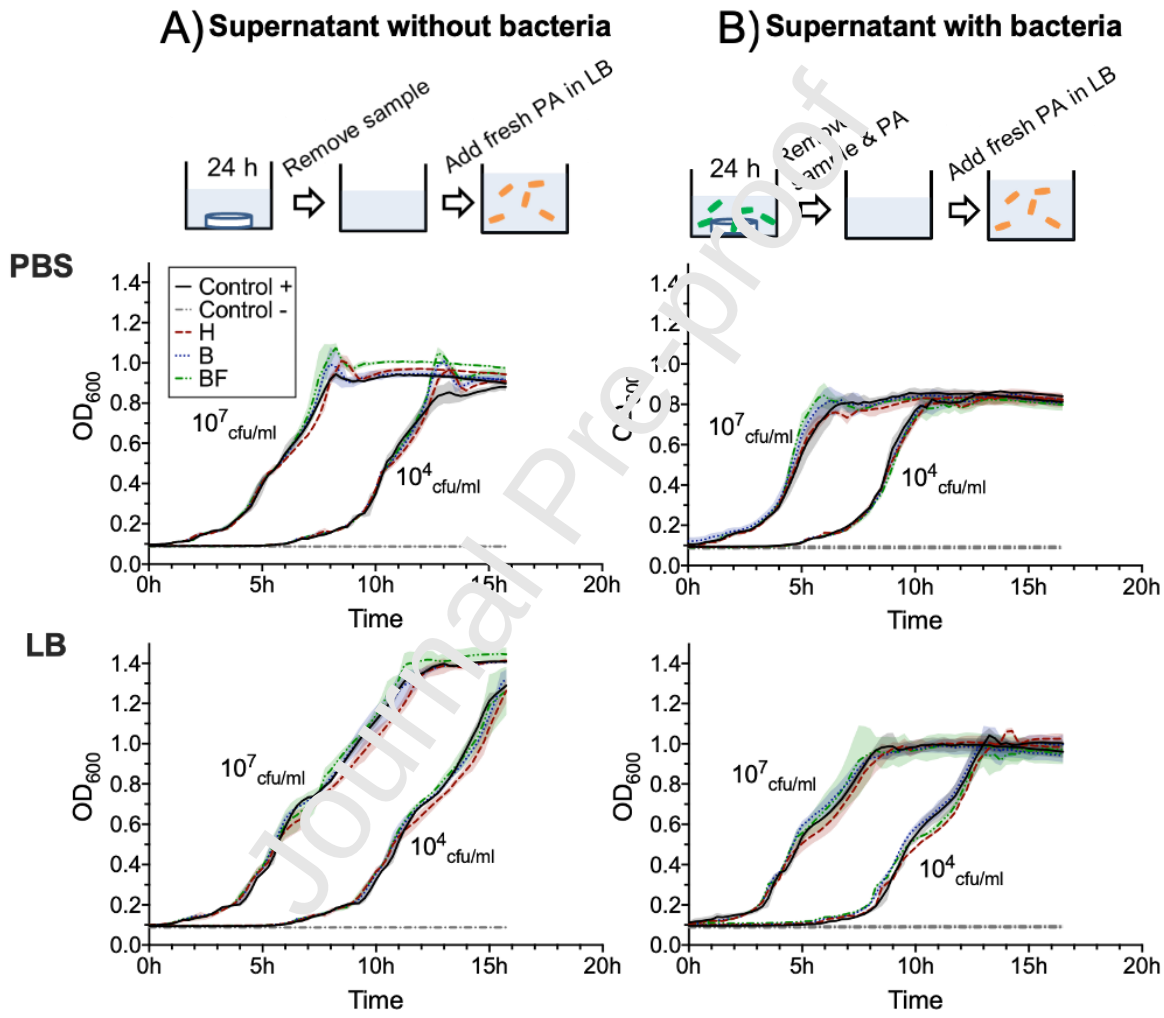

Figure 8. Growth curves monitored at 600 nm in PBS (a) and LB (b). Graphs from the first column correspond to supernatants of PBS and LB incubated for 24 h with the samples and subsequently filtered and supplemented with two different concentrations of fresh inoculum. Graphs from the second column correspond to supernatants of PBS and LB incubated for 24 h with the samples and P. aeruginosa and subsequently filtered and supplemented with two different concentrations of fresh inoculum. Positive controls correspond to incubation of bacteria with supernatant in which no sample was added. Negative controls correspond to incubation in PBS/LB without bacteria. Coloured shades correspond to the standard deviation of 3 measurements.

CONCLUSIONS

In this work, we reported the bactericidal potential of two different CDHA nanopillar substrates (B and F) prepared through simple and robust strategies based on the hydrolysis of α-TCP. By controlling the starting size of α-TCP and the consolidation conditions, the size, distribution, and density of the pillars were easily controlled. We further proved that the CDHA nanopillars were bactericidal with a lethality of up to 75% for the C substrate and 60% for F after 24 h incubation in PBS. This lethality was reduced to 20% for the flat control sample (BF). Importantly, the lethality of the nanopillared substrates depended on the type of medium used for the incubation of bacteria. In the absence of nutrients (in phosphate-buffered saline solution) more bacteria adhered (20% surface coverage) and adhesion was stronger, leading to higher lethality. However, in Luria broth (nutrient-containing medium) bacteria were less likely to adhere (5% surface coverage) and lower lethality was observed. The different substrates exhibited different degrees of reactivity, as observed by the levels of Ca and P ions in solution. Yet, the overall ionic exchanges in the solutions were not toxic to the planktonic cells. In view of this, we conclude that the main contributor to cell death was topography.

Declaration of Competing Interest

The authors declare that they have no known competing financial interests or personal relationships that could have appeared to influence the work reported in this document.

Acknowledgments

The authors acknowledge the Spanish Government for financial support through PID2019-103892RB-I00 project. They also thank the Generalitat the Catalunya for funding through projects 2017SGR-1165 and BASE3D 2021-P-001646 (co-funded by the European Regional Development Fund), as well as the ICREA Academia award of MPG, the FPI-MEC scholarship of MI and the Serra Hunter Program of IME. JMS benefits from a Marie Skłodowska-Curie Individual Fellowships from the European Commission through the H2020 project GAMBBa (Project ID: 892389).

References

[1] A.H. Schmidt, Autologous bone graft: Is it still the gold standard?, Injury. 52 (2021) S18–S22. https://doi.org/10.1016/j.injury.2021.01.043.
[2] World Health Organization, Global Guidelines for the Prevention of Surgical Site Infection, 2016.
[3] J.A. Wright, S.P. Nair, Interaction of staphylococci with bone, Int. J. Med. Microbiol. 300 (2010) 193–204. https://doi.org/10.1016/j.ijmm.2009.10.003.
[4] J. Hatzenbuehler, T.J. Pulling, Diagnosis and management of osteomyelitis, Am. Fam. Physician. 84 (2011) 1027–1033. https://doi.org/10.2165/00019053-199916060-00003.
[5] T. Strateva, D. Yordanov, Pseudomonas aeruginosa - A phenomenon of bacterial resistance, J. Med. Microbiol. 58 (2009) 1133–1148. https://doi.org/10.1099/jmm.0.009142-0.
[6] L.O. Conterno, M.D. Turchi, Antibiotics for treating chronic osteomyelitis in adults, Cochrane Database Syst. Rev. 2013 (2013). https://doi.org/10.1002/14651858.CD004439.pub3.
[7] C. Uruén, G. Chopo-Escuin, J. Tommassen, R.C. Mainar-Jaime, J. Arenas, Biofilms as promoters of bacterial

antibiotic resistance and tolerance, Antibiotics. 10 (2021) 1–36. https://doi.org/10.3390/antibiotics10010003.
[8] P.S. Stewart, J.W. Costerton, Antibiotic resistance of bacteria in biofilms, Lancet. 358 (2001) 135–138. https://doi.org/10.1016/S0140-6736(01)05321-1.
[9] Pr. Shankar, Book review: Tackling drug-resistant infections globally, Arch. Pharm. Pract. 7 (2016) 110. https://doi.org/10.4103/2045-080x.186181.
[10] A. Tagliabue, R. Rappuoli, Changing priorities in vaccinology: Antibiotic resistance moving to the top, Front. Immunol. 9 (2018) 1–9. https://doi.org/10.3389/fimmu.2018.01068.
[11] R.C. Moellering, NDM-1 — A Cause for Worldwide Concern, N. Engl. J. Med. 363 (2010) 2377–2379. https://doi.org/10.1056/nejmp1011715.
[12] J.S. Lee, W.L. Murphy, Functionalizing calcium phosphate biomaterials with antibacterial silver particles, Adv. Mater. 25 (2013) 1173–1179. https://doi.org/10.1002/adma.201203370.
[13] A. Ewald, D. Hösel, S. Patel, L.M. Grover, J.E. Barralet, U. Gbureck, Silver-doped calcium phosphate cements with antimicrobial activity, Acta Biomater. 7 (2011) 4064–4070. https://doi.org/10.1016/j.actbio.2011.06.049.
[14] A. Bensalem, O.K. Kucukosman, J. Raszkiewicz, F. Topkaya, Synthesis, characterization, bactericidal activity, and mechanical properties of hydroxyapatite nano powders impregnated with silver and zinc oxide nanoparticles (Ag-ZnO-Hap), Ceram. Int. 47 (2021) 21319–21324. https://doi.org/10.1016/j.ceramint.2021.04.139.
[15] A.A. Ivanova, R.A. Surmenev, M.A. Surmeneva, T. Mukhametkaliyev, K. Loza, O. Prymak, M. Epple, Hybrid biocomposite with a tunable antibacterial activity and bioactivity based on RF magnetron sputter deposited coating and silver nanoparticles, Appl. Surf. Sci. 329 (2015) 212–218. https://doi.org/10.1016/j.apsusc.2014.12.153.
[16] A. Tripathy, P. Sen, B. Su, W.H. Briscoe, Natural and bioinspired nanostructured bactericidal surfaces, Adv. Colloid Interface Sci. 248 (2017) 85–104. https://doi.org/10.1016/j.cis.2017.07.030.
[17] K. Modaresifar, S. Azizian, M. Ganjian, L.E. Fratila-Apachitei, A.A. Zadpoor, Bactericidal effects of nanopatterns: A systematic review, Acta Biomater. 83 (2019) 29–36. https://doi.org/10.1016/j.actbio.2018.09.059.
[18] D.P. Linklater, V.A. Baulin, S. Juodkazis, R.J. Crawford, P. Stoodley, E.P. Ivanova, Mechano-bactericidal actions of nanostructured surfaces, Nat. Rev. Microbiol. 19 (2021) 8–22. https://doi.org/10.1038/s41579-020-0414-z.
[19] J. Meng, P. Zhang, S. Wang, Recent progress in biointerfaces with controlled bacterial adhesion by using chemical and physical methods, Chem. - An Asian J. 9 (2014) 2004–2016. https://doi.org/10.1002/asia.201402200.
[20] E.P. Ivanova, J. Hasan, H.K. Webb, V.K. Truong, G.S. Watson, J.A. Watson, V.A. Baulin, S. Pogodin, J.Y. Wang, M.J. Tobin, C. Löbbe, R.J. Crawford, Natural bactericidal surfaces: Mechanical rupture of pseudomonas aeruginosa cells by cicada wings, Small. 8 (2012) 2489–2494. https://doi.org/10.1002/smll.201200528.
[21] E.P. Ivanova, J. Hasan, H.K. Webb, G. Gervinskas, S. Juodkazis, V.K. Truong, A.H.F. Wu, R.N. Lamb, V.A. Baulin, G.S. Watson, J.A. Watson, D.E. Mainwaring, R.J. Crawford, Bactericidal activity of black silicon, Nat. Commun. 4 (2013) 1–7. https://doi.org/10.1038/ncomms3838.
[22] J.M. Sadowska, K.J. Genderad, D.J. Kelly, F.J. O'Brien, Bone biomaterials for overcoming antimicrobial resistance: Advances in non-antibiotic antimicrobial approaches for regeneration of infected osseous tissue, Mater. Today. 46 (2021) 136–154. https://doi.org/10.1016/j.mattod.2020.12.018.
[23] J. Hasan, S. Raj, L. Yadav, K. Chatterjee, Engineering a nanostructured "super surface" with superhydrophobic and superkilling properties, RSC Adv. 5 (2015) 44953–44959. https://doi.org/10.1039/c5ra05206h.
[24] S. Pogodin, J. Hasan, V.A. Baulin, H.K. Webb, V.K. Truong, T.H. Phong Nguyen, V. Boshkovikj, C.J. Fluke, G.S. Watson, J.A. Watson, R.J. Crawford, E.P. Ivanova, Biophysical model of bacterial cell interactions with nanopatterned cicada wing surfaces, Biophys. J. 104 (2013) 835–840. https://doi.org/10.1016/j.bpj.2012.12.046.
[25] C.M. Bhadra, V. Khanh Truong, V.T.H. Pham, M. Al Kobaisi, G. Seniutinas, J.Y. Wang, S. Juodkazis, R.J. Crawford, E.P. Ivanova, Antibacterial titanium nano-patterned arrays inspired by dragonfly wings, Sci. Rep. 5 (2015) 1–12. https://doi.org/10.1038/srep16817.
[26] R. Fraioli, P.M. Tsimbouri, L.E. Fisher, A.H. Nobbs, B. Su, S. Neubauer, F. Rechenmacher, H. Kessler, M.P. Ginebra, M.J. Dalby, J.M. Manero, C. Mas-Moruno, Towards the cell-instructive bactericidal substrate: Exploring the combination of nanotopographical features and integrin selective synthetic ligands, Sci. Rep. 7 (2017) 1–14. https://doi.org/10.1038/s41598-017-16385-3.
[27] P.M. Tsimbouri, L. Fisher, N. Holloway, T. Sjostrom, A.H. Nobbs, R.M.D. Meek, B. Su, M.J. Dalby, Osteogenic and bactericidal surfaces from hydrothermal titania nanowires on titanium substrates, Sci. Rep. 6 (2016) 1–12. https://doi.org/10.1038/srep36857.
[28] D.W. Green, K.K.H. Lee, J.A. Watson, H.Y. Kim, K.S. Yoon, E.J. Kim, J.M. Lee, G.S. Watson, H.S. Jung, High Quality Bioreplication of Intricate Nanostructures from a Fragile Gecko Skin Surface with Bactericidal

Properties, Sci. Rep. 7 (2017) 1–12. https://doi.org/10.1038/srep41023.
[29] F. Viela, I. Navarro-Baena, A. Jacobo-Martín, J.J. Hernández, M. Boyano-Escalera, M.R. Osorio, I. Rodríguez, Nano-engineering safer-by-design nanoparticle based moth-eye mimetic bactericidal and cytocompatible polymer surfaces, RSC Adv. 8 (2018) 22606–22616. https://doi.org/10.1039/c8ra03403f.
[30] G. Tullii, S. Donini, C. Bossio, F. Lodola, M. Pasini, E. Parisini, F. Galeotti, M.R. Antognazza, Micro- and Nanopatterned Silk Substrates for Antifouling Applications, ACS Appl. Mater. Interfaces. 12 (2020) 5437–5446. https://doi.org/10.1021/acsami.9b18187.
[31] H.S. Sohn, J.K. Oh, Review of bone graft and bone substitutes with an emphasis on fracture surgeries, Biomater. Res. 23 (2019) 4–10. https://doi.org/10.1186/s40824-019-0157-y.
[32] W. Wang, K.W.K. Yeung, Bone grafts and biomaterials substitutes for bone defect repair: A review, Bioact. Mater. 2 (2017) 224–247. https://doi.org/10.1016/J.BIOACTMAT.2017.05.007.
[33] M.P. Ginebra, F.C.M. Driessens, J.A. Planell, Effect of the particle size on the micro and nanostructural features of a calcium phosphate cement: A kinetic analysis, Biomaterials. 25 (2004) 3453–3462.
[34] J.-M. Sadowska, J. Guillem-Marti, E.B. Montufar, M. Espanol, M.-P. Ginebra, Biomimetic versus sintered calcium phosphates: The in vitro behavior of osteoblasts and mesenchymal stem cells, Tissue Eng. - Part A. 23 (2017). https://doi.org/10.1089/ten.tea.2016.0406.
[35] A. Barba, A. Diez-Escudero, M. Espanol, M. Bonany, J.M. Sadowska, J. Guillem-Marti, C. Öhman-Mägi, C. Persson, M.-C. Manzanares, J. Franch, M.-P. Ginebra, The impact of biomimicry in the design of osteoinductive bone substitutes: nanoscale matters, ACS Appl. Mater. Interfaces. (2019) acsami.8b20749. https://doi.org/10.1021/acsami.8b20749.
[36] G. Bhardwaj, H. Yazici, T.J. Webster, Reducing bacteria and macrophage density on nanophase hydroxyapatite coated onto titanium surfaces without releasing pharmaceutical agents, Nanoscale. 7 (2015) 8416–8427. https://doi.org/10.1039/C5NR00471C.
[37] X. zhang, B. Wang, L. Ma, L. Xie, H. Yang, Y. Li, S. Wang, H. Qiao, H. Lin, J. Lan, Y. Huang, Chemical stability, antibacterial and osteogenic activities study of strontium-silver co-substituted fluorohydroxyapatite nanopillars: A potential multifunctional biological coating, Ceram. Int. 46 (2020) 27758–27773. https://doi.org/10.1016/j.ceramint.2020.07.275.
[38] E. Vidal, J. Guillem-Marti, M.P. Ginebra, C. Combes, E. Rupérez, D. Rodriguez, Multifunctional homogeneous calcium phosphate coatings: Toward antibacterial and cell adhesive titanium scaffolds, Surf. Coatings Technol. 405 (2021). https://doi.org/10.1016/j.surfcoat.2020.126557.
[39] C. Rey, C. Combes, C. Drouet, D. Grossin, G. Bertrand, J. Soulié, Bioactive calcium phosphate compounds: Physical chemistry, 2017. https://doi.org/10.1016/B978-0-12-803581-8.10171-7.
[40] J. Konka, M. Espanol, B.M. Bosch, E. de Oliveira, M.-P. Ginebra, Maturation of biomimetic hydroxyapatite in physiological fluids: a physicochemical and proteomic study, Mater. Today Bio. (2021) 100137. https://doi.org/10.1016/j.mtbio.2021.100137.
[41] J.-M. Sadowska, J. Guillem-Marti, E.B. Montufar, M. Espanol, M.-P. Ginebra, Biomimetic Versus Sintered Calcium Phosphates: The In Vitro Behavior of Osteoblasts and Mesenchymal Stem Cells, Tissue Eng. Part A. 23 (2017) 1297–1309. https://doi.org/10.1089/ten.tea.2016.0406.
[42] R.J. Crawford, H.K. Webb, V.K. Truong, J. Hasan, E.P. Ivanova, Surface topographical factors influencing bacterial attachment, Adv. Colloid Interface Sci. 179–182 (2012) 142–149. https://doi.org/10.1016/j.cis.2012.06.015.
[43] N. Doebelin, R. Kleeberg, Profex: a graphical user interface for the Rietveld refinement program BGMN, J. Appl. Cryst. 48 (2015) 1573–1580. https://doi.org/10.1107/S1600576715014685.
[44] X. Zhang, L. Wang, E. Levänen, Superhydrophobic surfaces for the reduction of bacterial adhesion, RSC Adv. 3 (2013) 12003–12020. https://doi.org/10.1039/c3ra40497h.
[45] M. Iafisco, A. Ruffini, A. Adamiano, S. Sprio, A. Tampieri, Biomimetic magnesium-carbonate-apatite nanocrystals endowed with strontium ions as anti-osteoporotic trigger, Mater. Sci. Eng. C. 35 (2014) 212–219. https://doi.org/10.1016/j.msec.2013.11.009.
[46] A. Ruffini, S. Sprio, L. Preti, A. Tampieri, Synthesis of Nanostructured Hydroxyapatite via Controlled Hydrothermal Route, in: R.S. and T.K. Mike Barbeck, Ole Jung (Ed.), Biomater. Tissue Reconstr. or Regen., IntechOpen, 2019: p. 13. https://doi.org/DOI: http://dx.doi.org/10.5772/intechopen.85091.
[47] Y. Raymond, M. Bonany, C. Lehmann, E. Thorel, R. Benítez, J. Franch, M. Espanol, X. Solé-Martí, M.-C. Manzanares, C. Canal, M.-P. Ginebra, Hydrothermal processing of 3D-printed calcium phosphate scaffolds enhances bone formation in vivo: a comparison with biomimetic treatment, Acta Biomater. (2021). https://doi.org/10.1016/j.actbio.2021.09.001.
[48] Q. Cui, T. Liu, X. Li, K. Song, D. Ge, Nanopillared Polycarbonate Surfaces Having Variable Feature Parameters as Bactericidal Coatings, ACS Appl. Nano Mater. 3 (2020) 4599–4609. https://doi.org/10.1021/acsanm.0c00645.

[49] M. Michalska, R. Divan, P. Noirot, P.D. Laible, Antimicrobial properties of nanostructured of surfaces – demonstrating the need for a standard, (2021). https://doi.org/10.1039/d1nr02953c.

[50] T.R. Thomas, Rough Surfaces Second Edition, Second Edi, Imperial College Press, London SW7 2BT, 1982.

[51] M.P. Ginebra, E. Fernandez, E.A. De Maeyer, R.M. Verbeeck, M.G. Boltong, J. Ginebra, F.C. Driessens, J.A. Planell, Setting Reaction and Hardening of an Apatitic Calcium Phosphate Cement, J. Biomater. Appl. 76 (1997) 905–912. https://doi.org/10.1177/0022034597076004120l.

[52] C. Rey, O. Marsan, C. Combes, C. Drouet, D. Grossin, S. Sarda, Characterization of Calcium Phosphates Using Vibrational Spectroscopies, 2014. https://doi.org/10.1007/978-3-642-53980-0_8.

[53] M. Markovic, B.O. Fowler, Preparation and Comprehensive Characterization of a Calcium Hydroxyapatite Reference Material, J. Res. Natl. Inst. Stand. Technol. 109 (2004) 553–568.

[54] L. Galea, D. Alexeev, M. Bohner, N. Doebelin, A.R. Studart, C.G. Aneziris, T. Graule, Textured and hierarchically structured calcium phosphate ceramic blocks through hydrothermal treatment, Biomaterials. 67 (2015) 93–103. https://doi.org/10.1016/j.biomaterials.2015.07.026.

[55] S. Gallinetti, C. Canal, M.-P. Ginebra, J. Ferreira, Development and Characterization of Biphasic Hydroxyapatite/β-TCP Cements., J. Am. Ceram. Soc. 97 (2014) 1065–1073. https://doi.org/10.1111/jace.12861.

[56] J. Sjollema, S.A.J. Zaat, V. Fontaine, M. Ramstedt, R. Luginbuehl, K. Thevissen, J. Li, H.C. van der Mei, H.J. Busscher, In vitro methods for the evaluation of antimicrobial surface designs, Acta Biomater. 70 (2018) 12–24. https://doi.org/10.1016/j.actbio.2018.02.001.

[57] E. Frimmersdorf, S. Horatzek, A. Pelnikevich, L. Wiehlmann, D. Schomburg, How Pseudomonas aeruginosa adapts to various environments: A metabolomic approach, Environ. Microbiol. 12 (2010) 1734–1747. https://doi.org/10.1111/j.1462-2920.2010.02253.x.

[58] C.H. Liao, L.M. Shollenberger, Survivability and long-term preservation of bacteria in water and in phosphate-buffered saline, Lett. Appl. Microbiol. 37 (2003) 45–50. https://doi.org/10.1046/j.1472-765X.2003.01345.x.

[59] A. Elbourne, V.E. Coyle, V.K. Truong, Y.M. Sabri, A.E. Kandjani, S.K. Bhargava, E.P. Ivanova, R.J. Crawford, Multi-directional electrodeposited gold nanospikes for antibacterial surface applications, Nanoscale Adv. 1 (2019) 203–212. https://doi.org/10.1039/c8na00124c.

[60] V.T.H. Pham, V.K. Truong, M.D.J. Quinn, S.M. Notley, Y. Guo, V.A. Baulin, M. Al Kobaisi, R.J. Crawford, E.P. Ivanova, Graphene Induces Formation of Pores That Kill Spherical and Rod-Shaped Bacteria, ACS Nano. 9 (2015) 8458–8467. https://doi.org/10.1021/acsnano.5b03368.

[61] X. Wang, C.M. Bhadra, T.H. Yen Dang, R. Buividas, J. Wang, R.J. Crawford, E.P. Ivanova, S. Juodkazis, A bactericidal microfluidic device constructed using nano-textured black silicon, RSC Adv. 6 (2016) 26300–26306. https://doi.org/10.1039/c6ra03864f.

[62] C.D. Bandara, S. Singh, I.O. Afara, A. Wolff, T. Tesfamichael, K. Ostrikov, A. Oloyede, Bactericidal Effects of Natural Nanotopography of Dragonfly Wing on Escherichia coli, ACS Appl. Mater. Interfaces. 9 (2017) 6746–6760. https://doi.org/10.1021/acsami.6b13666.

[63] R. Fontelo, D. Soares da Costa, F.L. Reis, R. Novoa-Carballal, I. Pashkuleva, Bactericidal nanopatterns generated by block copolymer self-assembly, Acta Biomater. 112 (2020) 174–181. https://doi.org/10.1016/j.actbio.2020.06.003.

[64] J. Hasan, R.J. Crawford, E.P. Ivanova, Antibacterial surfaces: The quest for a new generation of biomaterials, Trends Biotechnol. 31 (2013) 295–304. https://doi.org/10.1016/j.tibtech.2013.01.017.

[65] J. Li, Y. Zhang, J. Enhe, B. Yao, Y. Wang, D. Zhu, Z. Li, W. Song, X. Duan, X. Yuan, X. Fu, S. Huang, Bioactive nanoparticle reinforced alginate/gelatin bioink for the maintenance of stem cell stemness, Mater. Sci. Eng. C. 126 (2021) 112193. https://doi.org/10.1016/j.msec.2021.112193.

[66] A. Jaggessar, A. Mathew, H. Wang, T. Tesfamichael, C. Yan, P.K. Yarlagadda, Mechanical, bactericidal and osteogenic behaviours of hydrothermally synthesised TiO 2 nanowire arrays, J. Mech. Behav. Biomed. Mater. 80 (2018) 311–319. https://doi.org/10.1016/j.jmbbm.2018.02.011.

[67] S. Kjelleberg, B.A. Humphrey, K.C. Marshall, Initial Phases of Starvation and Activity of Bacteria at Surfaces, Appl. Environ. Microbiol. 46 (1983) 978–984. https://doi.org/10.1128/aem.46.5.978-984.1983.

[68] A. Hayles, J. Hasan, R. Bright, D. Palms, T. Brown, D. Barker, K. Vasilev, Hydrothermally etched titanium: a review on a promising mechano-bactericidal surface for implant applications, Mater. Today Chem. 22 (2021) 100622. https://doi.org/10.1016/j.mtchem.2021.100622.

[69] M. Köller, N. Ziegler, C. Sengstock, T.A. Schildhauer, A. Ludwig, Bacterial cell division is involved in the damage of gram-negative bacteria on a nano-pillar titanium surface, Biomed. Phys. Eng. Express. 4 (2018). https://doi.org/10.1088/2057-1976/aad2c1.

[70] C. Sengstock, M. Lopian, Y. Motemani, A. Borgmann, C. Khare, P.J.S. Buenconsejo, T.A. Schildhauer, A. Ludwig, M. Köller, Structure-related antibacterial activity of a titanium nanostructured surface fabricated by glancing angle sputter deposition, Nanotechnology. 25 (2014). https://doi.org/10.1088/0957-4484/25/19/195101.

[71] F. Hizal, C.H. Choi, H.J. Busscher, H.C. Van Der Mei, Staphylococcal Adhesion, Detachment and Transmission on Nanopillared Si Surfaces, ACS Appl. Mater. Interfaces. 8 (2016) 30430–30439. https://doi.org/10.1021/acsami.6b09437.
[72] N. Lin, P. Berton, C. Moraes, R.D. Rogers, N. Tufenkji, Nanodarts, nanoblades, and nanospikes: Mechano-bactericidal nanostructures and where to find them, Adv. Colloid Interface Sci. 252 (2018) 55–68. https://doi.org/10.1016/j.cis.2017.12.007.
[73] L. Hanson, Z.C. Lin, C. Xie, Y. Cui, B. Cui, Characterization of the cell-nanopillar interface by transmission electron microscopy, Nano Lett. 12 (2012) 5815–5820. https://doi.org/10.1021/nl303163y.
[74] K. Myszka, K. Czaczyk, Characterization of adhesive exopolysaccharide (EPS) produced by Pseudomonas aeruginosa under starvation conditions, Curr. Microbiol. 58 (2009) 541–546. https://doi.org/10.1007/s00284-009-9365-3.
[75] J.M. Schierholz, J. Beuth, Implant infections: A haven for opportunistic bacteria, J. Hosp. Infect. 49 (2001) 87–93. https://doi.org/10.1053/jhin.2001.1052.
[76] G. Kalayu, Phosphate solubilizing microorganisms: Promising approach as biofertilizers, Int. J. Agron. 2019 (2019). https://doi.org/10.1155/2019/4917256.
[77] A. Buch, G. Archana, G. Naresh Kumar, Metabolic channeling of glucose towards gluconate in phosphate-solubilizing Pseudomonas aeruginosa P4 under phosphorus deficiency, Res. Microbiol. 159 (2008) 635–642. https://doi.org/10.1016/j.resmic.2008.09.012.
[78] A.H. Goldstein, Recent progress in understanding the molecular genetics and biochemistry of calcium phosphate solubilization by gram negative bacteria, Biol. Agric. Hortic. 12 (1995) 185–193. https://doi.org/10.1080/01448765.1995.9754736.
[79] S. Cazalbou, C. Combes, D. Eichert, C. Rey, M.J. Glimcher, Poorly crystalline apatites: Evolution and maturation in vitro and in vivo, J. Bone Miner. Metab. 22 (2004) 310–317. https://doi.org/10.1007/s00774-004-0488-0.
[80] C. Rey, C. Combes, C. Drouet, H. Sfihi, a. Barroug, Physico-chemical properties of nanocrystalline apatites: Implications for biominerals and biomaterials, Mater. Sci. Eng. C. 27 (2007) 198–205. https://doi.org/10.1016/j.msec.2006.05.015.
[81] J. Gustavsson, M.P. Ginebra, J. Planell, E. Engel, Osteoblast-like cellular response to dynamic changes in the ionic extracellular environment produced by calcium-deficient hydroxyapatite, J. Mater. Sci. Mater. Med. 23 (2012) 2509–2520. https://doi.org/10.1007/s10856-012-4705-4.
[82] S. Samavedi, A.R. Whittington, A.S. Goldstein, Calcium phosphate ceramics in bone tissue engineering: A review of properties and their influence on cell behavior, Acta Biomater. 9 (2013) 8037–8045. https://doi.org/10.1016/j.actbio.2013.06.014.
[83] J. Gustavsson, M.P. Ginebra, E. Engel, J. Planell, Ion reactivity of calcium-deficient hydroxyapatite in standard cell culture media, Acta Biomater. 7 (2011) 4242–4252. https://doi.org/10.1016/j.actbio.2011.07.016.
[84] K.C. Marshall, B.L. Blainey, Role of Bacterial Adhesion in Biofilm Formation and Biocorrosion, in: Biofouling Biocorrosion Ind. Water Syst., 1991. pp. 29–46. https://doi.org/10.1007/978-3-642-76543-8_3.
[85] T. Rasamiravaka, Q. Labtani, P. Duez, andMondher El Jaziri, The Formation of Biofilms by Pseudomonas aeruginosa: A Review of the Natural and Synthetic Compounds Interfering with Control Mechanisms, Biomed Res. Int. 2015 (2015) 1–17.
[86] A.J. De Kerchove, M. Elimelech, Calcium and magnesium cations enhance the adhesion of motile and nonmotile Pseudomonas aeruginosa on alginate films, Langmuir. 24 (2008) 3392–3399. https://doi.org/10.1021/la7036229.
[87] E. Padan, E. Bibi, M. Ito, T.A. Krulwich, Alkaline pH homeostasis in bacteria: New insights, Biochim. Biophys. Acta - Biomembr. 1717 (2005) 67–88. https://doi.org/10.1016/j.bbamem.2005.09.010.
[88] K. Romanowski, A. Zaborin, H. Fernandez, V. Poroyko, V. Valuckaite, S. Gerdes, D.C. Liu, O.Y. Zaborina, J.C. Alverdy, Prevention of siderophore- mediated gut-derived sepsis due to P. aeruginosa can be achieved without iron provision by maintaining local phosphate abundance: Role of pH, BMC Microbiol. 11 (2011) 212. https://doi.org/10.1186/1471-2180-11-212.
[89] A.J. Bullock, M. Garcia, J. Shepherd, I. Rehman, M. Sheila, Bacteria induced pH changes in tissue-engineered human skin detected non-invasively using Raman confocal spectroscopy, Appl. Spectrosc. Rev. 55 (2020) 158–171. https://doi.org/10.1080/05704928.2018.1558232.
[90] A. Junka, P. Szymczyk, G. Ziółkowski, E. Karuga-Kuzniewska, D. Smutnicka, I. Bil-Lula, M. Bartoszewicz, S. Mahabady, P.P. Sedghizadeh, Bad to the bone: On in vitro and ex vivo microbial biofilm ability to directly destroy colonized bone surfaces without participation of host immunity or osteoclastogenesis, PLoS One. 12 (2017) 1–20. https://doi.org/10.1371/journal.pone.0169565.

CRediT authorship contribution statement

Marc Iglesias-Fernandez: Investigation, Methodology, Formal analysis, Visualization, Writing – original draft. **Judit Buxadera-Palomero:** Investigation, Validation. **Joanna-Maria Sadowska:** Investigation, Review. **Montserrat Espanol:** Conceptualization, Investigation, Supervision, Writing – review & editing. **Maria Pau Ginebra:** Conceptualization, Resources, Writing – review & editing.

Highlights:

- Nanopatterned topographies on calcium phosphates can kill bacteria
- Different nanopatterns show different degrees of bacteria mortality
- The incubation media has an impact on bacterial adhesion
- Ionic exchanges in calcium phosphates have a minor contribution to bacterial lethality